Computer vision–enabled evaluation of boom dynamics and application uniformity on commercial sprayers under real-world operating conditions.

by

Treman Singh Kaloya

B.Tech., Punjab Agricultural University, 2019

A THESIS

submitted in partial fulfillment of the requirements for the degree

MASTER OF SCIENCE

Carl and Melinda Helwig Department of Biological and Agricultural Engineering
Carl R. Ice College of Engineering

KANSAS STATE UNIVERSITY
Manhattan, Kansas

2025

Approved by:

Major Professor
Dr. Ajay Sharda

Copyright

© Treman Kaloya 2025.

Abstract

Efficient and uniform spraying is one of the biggest challenges in modern crop production. As sprayer booms get wider and machines travel faster, even small vibrations or terrain changes can disturb how chemicals reach the crop canopy. When a nozzle moves too far ahead or behind, or rises and dips too much, the spray pattern shifts—causing some areas to be under-applied and others over-applied. These subtle height and motion changes, though often invisible during operation, have a major impact on coverage, drift, and chemical waste.

This research combined field experiments, computer vision, and advanced sensing to understand how a 120-ft sprayer boom moves and how that motion affects spraying accuracy under real field conditions. A computer vision Distance Quantifier System (DQS) Dalal et al., (2025) was developed to track a reflective fiducial target mounted on the boom tip. The system, paired with a dual-frequency GNSS receiver, recorded motion at 10 Hz with centimeter-level precision. In the first phase, this DQS–GNSS framework was used to measure horizontal (fore–aft) boom motion and its impact on chemical application rate for three commercial self-propelled sprayers: a Hagie STS12 (front boom, hybrid aluminum–steel truss), a John Deere 412R (rear boom, steel truss), and a Miller Nitro 7310 (front boom, steel truss).

Field trials conducted across approximately 100 acres demonstrated that horizontal surging resulted in localized under- and over-application, even when rate controllers maintained the target flow. Among the three machines, the rear-boom John Deere remained the most stable (≤ 2 % rate-error exceedance area at the 10 % rate-error threshold), while Miller's heavier all-steel front boom displayed the largest fore–aft excursions—reaching up to 2.7 m—and the highest rate-error exceedance area (7–10 %). The hybrid Hagie (Steel + Aluminum boom) showed intermediate behavior. Statistical analysis confirmed that boom design—specifically, position, material, and mass distribution—had a significantly stronger effect on rate uniformity than travel speed, which had only a minor scaling influence. These results provided the first field-scale evidence linking horizontal boom motion directly to measurable rate error.

In the second phase, the framework was expanded to include radar canopy sensors alongside the existing DQS–GNSS setup, enabling simultaneous measurement of boom motion and canopy surface response. Using a New Holland Guardian SF310 – a 120ft front-boom sprayer with synchronized DQS, GNSS, and company-fitted Raven AutoBoom XRT radars were used to reconstruct nozzle-to-canopy clearances along the 60-ft left wing. Results revealed that vertical

motion was dominated by rigid-body pitching about the boom hinge rather than terrain following. The boom often tilted more than 3°, occasionally exceeding 4.8°, with corresponding tip displacements up to 1.07 m. Strong correlations ($r > 0.85$) between tip and mid-radar signals confirmed coherent canopy undulations across the boom span. Fault analysis showed that both the frequency and magnitude of height deviations increased with travel speed and with lateral distance from the hinge. At the strict ±5 in (±0.127 m) tolerance, the left boom wing operated outside the target height for about 37 % of the run at 6 mph, 41 % at 12 mph, and 44 % at 18 mph. When the tolerance was relaxed to ±10 in (±0.254 m), these out-of-tolerance-time fractions were reduced by roughly half. The tip section, being farthest from the hinge, consistently exhibited the largest deviation—exceeding 59 % rate error exceedance under the tighter ±5 in band—while the center section remained the most stable. When a height-based section shut-off logic (+27in /-20in) was applied, the system predicted an average 10 % reduction in active spray time, equivalent to nearly 5 L of chemical savings per boom per pass, or more than 35 L per 100 acres of field coverage.

Overall, this research demonstrated that both horizontal and vertical instabilities significantly influence spray uniformity. Together, the two studies show how complementary sensing of boom motion and canopy profile can be used to quantify field-scale spraying stability. The integrated DQS–GNSS–radar framework developed through this research provides a practical foundation for future adaptive control systems and sprayer designs aimed at improving application uniformity, chemical efficiency, and drift reduction.

Table of Contents

List of Figures viii
List of Tables x
Acknowledgements xi
Chapter 1 - Introduction 1
1.1 Background and Motivation 1
1.2 Limitations of Existing Boom Control Systems 1
1.3 Research Gaps 2
a). Boom dynamics, spray patterns, and height control 2
b). Dynamic modelling and active control 3
c). Overall gaps 4
1.4 Development of a Multi-Sensor Framework 4
1.5 Research Objectives 5
a). Phase 1: Horizontal Motion and Application Rate Error. 5
b). Phase 2: Vertical Motion and Nozzle-to-Canopy Clearance. 5
Chapter 2 - Impact of Horizontal Boom Motion on Application Rate Error: Field Evaluation of Three 120-Ft (36m) Sprayers 7
2.1 Abstract 7
2.2 Introduction 7
2.3 Materials & Methods 10
2.3.1 Distance Quantifier System 10
2.3.2 Experimental Site 11
2.3.3 Sprayers Tested 12
2.3.4 Test Protocol 12
2.3.5 Data Processing 13
2.3.6 Statistical Analysis 16
2.4 Results & Discussion 17
2.4.1 XY density scatter plot 17
2.4.2 Boom tip displacement 18
2.4.3 Instantaneous rate error 19
2.4.4 Rate-error exceedance boom area (dwell-qualified aggregation) 19

2.4.5 Nozzle-wise rate error exceedance 21
2.4.6 Sprayer vs sprayer comparisons 22
2.4.7 Statistical Validation 23
2.4.8 Sprayer Design Effects 24
2.5 Conclusion 25
Chapter 3 - Field-based evaluation of Vertical Motion and Canopy Clearance in a 120-Ft Sprayer Boom using synchronized DQS, GNSS, and Radar Sensors 27
3.1 Abstract 27
3.2 Introduction 28
3.3 Materials and Methods 29
3.3.1 Experimental setup 29
3.3.2 Sprayers Tested 30
3.3.3 Test Protocol 31
3.3.4 Sensors and instrumentation 31
3.3.5 Radar sensors accuracy check 32
3.3.6 Data Processing 33
a). Baseline reference (DQS initialization) 33
b). Sectional grouping of nozzles 33
c). Nozzle-to-canopy clearance modeling 35
3.3.7 Metrics and statistical analysis 35
a). Nozzle-level error classification 35
b). Section-level aggregation and Shut Off 36
c). Wing -Level aggregation and Additional motion metrics 37
3.4 Results & Discussion 37
3.4.1 DQS Tip Vertical Motion 37
3.4.2 Radar-Measured Canopy Profiles 39
3.4.3 Radar Cross-Correlation and Boom Motion Statistics 40
3.4.4 Tilt Angle Statistics 41
3.4.5 Section-Wise Height-tolerance exceedance 42
3.4.6 Section Shut Off Command 44
3.4.7 Wing-level height exceedance summaries 45

3.5 Conclusion 46
Chapter 4 - Conclusion 48
4.1 Summary of Findings 48
4.2 Practical Implications 49
4.3 Future Work 50
References 51

List of Figures

Figure 1: *Example of horizontal boom surge measured in the field. Blue line shows the GNSS track at the boom center; orange line shows the left boom tip path measured with the Distance Quantifier System (DQS). The sprayer image is illustrative. Forward surges increased nozzle ground speed, creating under-spray, while backward lags decreased speed and caused over-application. Direction of sprayer Right to Left.* 9

Figure 2: *Setup of the Distance Quantifier System (DQS) on the sprayer boom.* 10

Figure 3: *Planned and actual field trial paths for maneuver testing. (A) Prescribed track plan showing designated corridors for sprayer runs at 6, 12, and 18 mph, with practice run area indicated. (B) Example of an actual GNSS track from the John Deere 412R sprayer following the prescribed course. Disturbance zones included terraces, approaches, braking, acceleration, and turns, designed to excite fore–aft boom motion under realistic field conditions.* 13

Figure 4: *Boxplots of horizontal (Δx_tip meters) vs. vertical (Δz_tip meters) displacement for all sprayer × speed conditions. dashed circles ±5in /±10in ; crosshairs = stabilized (0,0) start, scatter points show raw displacement.* 17

Figure 5: *P95 and RMS fore–aft displacement for each sprayer × speed condition.* 19

Figure 6: *P95 |E| instantaneous application rate error by sprayer and speed.* 19

Figure 7: *Nozzle-wise rate error exceedance fractions for the 5%, 10%, and 15% thresholds across sprayers and travel speeds. Each panel shows the fraction of run time that each boom nozzle exceeded a given rate error threshold, with inverted triangles marking individual nozzle positions from hinge to tip. The horizontal red line marks a 10% persistence benchmark common to all sprayers. For each threshold, a color-matched vertical dotted line marks the first nozzle where the exceedance fraction reaches 10%, and the corresponding nozzle index annotated shows the nozzle crossing the 10 % line (for example, "Nozzle-25 in Hagie at 18 mph").* 21

Figure 8: *Rate-error exceedance boom area fractions at 5%, 10%, and 15% thresholds across speeds for each sprayer.* 22

Figure 9: *Sprayer Specimen - New Holland SF310* 30

Figure 10: *Setup of the Distance Quantifier System (DQS) on the sprayer boom. (1) Scutoid fiducial target mounted on the left boom tip; (2) DQS camera at the boom center; (3) GNSS-Topcon receiver at boom center; (4) Raven AutoBoom® XRT Radar sensor.* 32
Figure 11: *Sectional Grouping of nozzles.* 34
Figure 12: *Time-series of DQS-measured tip vertical displacement (Δz_tip) at three forward speeds (6, 12, 18 mph). The traces share a common vertical scale for comparison. The largest oscillation envelope occurs at 12 mph, indicating resonance-like amplification of boom response.* 37
Figure 13: XY *Scatterplots of DQS horizontal versus vertical displacement (Δx_tip vs Δz_tip) for 6, 12, and 18 mph. Shared axes ±1.524 m; dashed circles at ±0.127 m and ±0.254 m; crosshairs = stabilized (0,0) start.* 38
Figure 14: *Canopy distances recorded by the three radar sensors (tip, mid, centre) at 6,12 and 18mph in top row; bottom row shows the zoomed-in view for the same windows to aid curve separation(6 mph: 490–520 s; 12 mph: 260–280 s; 18 mph: 90–110 s).* 40
Figure 15: *Bar plots of section-wise height-tolerance exceedance (%) under tolerance bands of ±5" (±0.127 m) and ±10" (±0.254 m). Tip sections consistently exhibit higher time outside height tolerance across all speeds.* 43
Figure 16: *Section Shutt off % for nozzle sections(Tip, Mid, Centre).* 44
Figure 17: *Wing-level time outside height tolerance (%) versus speed under three tolerance thresholds (±5", ±10"). Fault percentage increases with speed and decreases as the band widens.* 45

List of Tables

Table 1: *Specifications of Sprayer model used in field trials* 12
Table 2: *Statistics Summary Table for rate-error exceedance boom area for the 3 sprayers.*..... 20
Table 3: *Two-way ANOVA results for rate-error exceedance area (≥10%).* 23
Table 4: *Tukey HSD post-hoc test (Sprayer, averaged over speeds).*..... 23
Table 5: *Tukey HSD post-hoc test (Speed, averaged over sprayers).*..... 24
Table 6: *Specifications of Sprayer model used in field trials.* 30
Table 7: *Statistic summary table of DQS vertical (Δz).* 38
Table 8: *Statistic summary table of Radar Sensors (Tip, Mid, Centre).*..... 39
Table 9: *Pearson correlations matrix summary table of Radar Sensors (Tip, Mid, Centre).* 41
Table 10: *Statistic summary table of Tilt angle θ°.*..... 41
Table 11: *Section-wise height-tolerance exceedance time (%) under ±5" and ±10" tolerance bands.* 42
Table 12: *% time each nozzle section operated outside the set height limits (+27"/-20").*..... 44
Table 13: *Wing % time outside height tolerance vs Speeds.*..... 45

Acknowledgements

I am profoundly grateful to my major professor, **Dr. Ajay Sharda**, for his unwavering guidance, high standards, and steady support from the first idea to the final draft. His mentorship shaped both this work and my approach to research. I also thank my committee members (**Dr. Andres Patrignani** and Dr. **Daniel Flippo**) for their time, thoughtful questions, and constructive feedback that strengthened this thesis.

My sincere appreciation goes to the entire **FARMS Lab** team for being there in the field and in the lab—early mornings, late nights, and everything in between. This project would not have been possible without the partnership and trust of our on-farm collaborators. Thank you, **Kyle**, for providing access to your fields and the Hagie and John Deere sprayers, and **Josh** for skillful and patient sprayer operation during data collection.

I am grateful to our collaborators at CNH Industrial, especially **Kevin Smith** and **Jeremy**, for coordinating logistics, sharing technical insights, and enabling access to the Miller and New Holland sprayers used in this study.

Special thanks to **Rahul Singh** for standing shoulder-to-shoulder with me through almost every trial and to **Sidharth** for his help with the computer-vision development for the DQS system. I also acknowledge **Benjamin** for fabricating the 3D mounts and **Jose** for building the DAQ box—your practical solutions kept the project moving when it mattered most.

Finally, I am thankful for the encouragement of friends and family, whose patience and belief sustained me through long days in the field and longer nights over datasets. To everyone who contributed time, tools, advice, or good humor—thank you. This thesis is as much yours as it is mine.

Chapter 1 - Introduction

1.1 Background and Motivation

Uniform and efficient spraying remains one of the most critical challenges in modern crop production. The goal of every spray operation is to apply the right chemical dose to the right place at the right time. However, achieving consistent spray coverage over large and variable fields is difficult. Even small variations in boom height, speed, or orientation can significantly affect how droplets reach the target surface. When a nozzle moves too far ahead or behind due to horizontal surge, or rises and dips excessively because of vertical oscillation, the spray pattern shifts—creating areas that are under-applied or over-applied. These inconsistencies reduce pest control efficacy, waste expensive chemicals, and increase the potential for off-target drift.

The importance of precise boom stability has increased with the rapid growth of high-capacity self-propelled sprayers. Modern machines often operate at speeds exceeding 25–30 km h^{-1} (15–18 mph) and are equipped with booms extending up to 36–48 m (120–160 ft). At such widths, the boom acts as a flexible beam that amplifies vibrations and ground disturbances. The challenge is further compounded by uneven terrain, headlands, terraces, and across-slope travel—all of which excite dynamic motion at the boom tips. These oscillations, though often imperceptible to the operator, translate directly into variations in nozzle height, velocity, and therefore local application rate.

Uniform spray distribution is not merely a mechanical concern; it directly affects chemical efficiency, canopy coverage, and environmental safety. Over-application leads to runoff, residue, and crop damage, while under-application promotes pest resistance and yield loss. Field studies have shown that non-uniformity resulting from boom motion can reduce deposition uniformity by more than 15% and cause visible streaking across crop rows (Anglund and Ayers, 2003);(Sharda et al. 2011). These issues highlight the need for accurate characterization of boom motion under true field conditions rather than controlled laboratory tests.

1.2 Limitations of Existing Boom Control Systems

To improve application uniformity, manufacturers have developed rate controllers and automatic boom-height control systems. Rate controllers adjust nozzle flow according to vehicle speed, while height controllers use ultrasonic or radar sensors to maintain a preset clearance above

the ground or canopy. Although these systems have improved average performance, they are inherently limited by response time and sensor accuracy.

Most rate controllers assume that every nozzle moves at the same ground speed as the vehicle's centerline unless the sprayer is taking a turn, and then they take the yaw angle into consideration. The boom tips experience additional forward–backward motion caused by acceleration, braking, and chassis pitching etc. This motion changes the instantaneous ground speed of individual nozzles, altering the effective spray dose even when the system maintains a steady flow rate *(Figure 1)*. Similarly, boom-height controllers rely on point-based ultrasonic measurements that may lag behind actual terrain undulations, particularly over rough or cross-slope fields. These controllers stabilize the average boom height but cannot fully eliminate the oscillations that occur along the span.

As a result, there remains a gap between what is controlled and what actually happens in the field. While sensors and control systems keep setpoints near their targets, the dynamic motion of the boom structure continues to cause local deviations in spray delivery. Quantifying these deviations under real-world conditions requires measurement tools capable of tracking both boom and canopy movement with high spatial and temporal resolution.

1.3 Research Gaps

Some studies focus on how the boom moves and how this affects spray patterns. Others focus on boom-height sensors and automatic height control. A third group uses computer models and simulations. Very few combine full-scale motion measurement on modern self-propelled sprayers with direct agronomic indicators such as rate error, faulty spraying time, or nozzle-to-canopy clearance.

a). Boom dynamics, spray patterns, and height control

Early dynamic studies showed clearly that boom motion affects spray uniformity. Nation et al., (1982) used accelerometers to measure how field sprayer booms move and found that chassis rotation and field roughness created large tip movements, especially near the boom ends. (Langenakens et al. 1995) and (Langenakens et al., 1999) combined experimental tests and modelling to study how horizontal and vertical movements change spray distribution. They showed that both directions of motion reduced uniformity and that tyre pressure, speed, and boom design influenced vibration levels and patterns. Later, (Ooms et al. 2003) and (Ooms et al. 2002) used a combination of accelerometers and ultrasonic sensors to separate different types of

horizontal boom motion (yaw, jolt, deformation), reconstruct boom displacement, and relate these movements to changes in longitudinal spray distribution in field conditions. (Pochi and Vannucci, 2002) designed a portable system with potentiometric transducers to record three-dimensional movement, velocity, and acceleration at two points on the boom and used these data as indicators of boom stability. Reynaldo et al., (2016) extended this to self-propelled sprayers using Real Time Kinematic Global Navigation Satellite System (RTK-GNSS) to measure vertical and horizontal oscillations and showed that motion levels depend on machine model, track profile, and speed.

A second line of work focuses on boom-height sensing and automatic height control. Zhao et al., (2022) developed an ultrasonic boom-height detection system for wheat and studied how well it measured boom-to-canopy distance at different growth stages. Dou et al., (2021) developed a single-point light detection and ranging (LiDAR) height sensor and showed that it can be more accurate and stable than ultrasonic sensors on rough surfaces. At the same time, (Herbst et al. 2015), and (Miles 2018) describe how to test boom steadiness and height-control performance using defined tracks, moving targets, and multiple height sensors, and how to compare different control systems.

Taken together, these studies firmly establish that boom dynamics and height control are important and that motion can distort spray patterns. They also provide tools to measure local height and to test control systems. However, they mostly use shorter booms or controlled tracks, instrument only a few points, and report results as displacement, vibration levels, or broad uniformity indices. They do not provide continuous, nozzle-level motion and clearance on a 36.6 m boom in real fields, and they do not express the impact in terms of instantaneous rate error, rate-error exceedance area, time outside a defined nozzle-to-canopy height band, or field-scale faulty spraying time and chemical savings.

b). Dynamic modelling and active control

More recent studies use dynamic modelling and active control to predict and reduce boom motion. Yan et al., (2021) built a mathematical model of a spray boom using masses, springs, and dampers and analysed how boom design and suspension properties affect vibration when the sprayer encounters a step-like disturbance. Bockhop et al., (2024) studied an off-road hydraulic lift arm suspension and showed how suspension settings influence vertical motion in rough terrain, with clear implications for mounted implements such as booms. Tahmasebi et al., (2012) designed an active suspension strategy for sprayer booms using an intelligent Active Force Control (AFC)

scheme with Proportional–Integral–Derivative (PID) control and showed in simulation that this reduced boom vibration more than conventional control.

These modelling and control studies are valuable for design because they show how changes in structure and control can reduce motion. But they are mostly simulation-based and are validated with limited sensor data. Their outputs are expressed in mechanical terms (displacement, acceleration, mode shapes) and do not include measured full-scale boom motion in real fields or derived agronomic metrics such as rate error, faulty time, or clearance-based shut-off performance.

c). Overall gaps

From this body of work, three main gaps remain:

1. Most experiments were conducted on short booms (< 6 m) or smooth test tracks, which fail to reproduce the complexity of field conditions involving terraces, ruts, and cross-slope disturbances.
2. These studies advanced understanding of mechanical behavior but rarely linked measured motion to practical spraying outcomes such as rate error, rate-error exceedance area, or canopy clearance deviation.
3. Height-sensing and control studies typically measure distance at a few points for control purposes. They do not simultaneously capture boom kinematics and canopy height along the whole boom, so they cannot reconstruct nozzle-level clearances or distinguish whether a deviation came from boom dynamics, canopy variation, or both.

Therefore, there is a clear need for a field-based, high-precision sensing framework that can capture true boom motion in both horizontal and vertical directions and directly connect it to spraying accuracy and agronomic performance.

1.4 Development of a Multi-Sensor Framework

To address these limitations, this research developed a novel sensing platform integrating computer vision, dual-frequency GNSS, and radar canopy sensors. The central innovation was the Distance Quantifier System (DQS) (mentioned in 2.3.1) — a camera-based computer-vision tool capable of tracking a reflective fiducial marker mounted on the boom tip. The DQS captured tip displacement at 10 Hz with centimeter-level accuracy and was synchronized with GNSS signals providing vehicle speed and elevation data.

In the second stage, radar canopy sensors were incorporated to measure canopy surface height under the boom, enabling simultaneous evaluation of boom motion and canopy response.

The combined DQS–GNSS–radar framework thus offered a complete picture of how the boom moves relative to both the sprayer chassis and the ground surface, providing data necessary for reconstructing nozzle-to-canopy clearances across the span.

This framework enabled a new class of analyses: it allowed dynamic boom displacement to be converted into meaningful agronomic metrics such as instantaneous rate error, height-tolerance exceedance duration, and potential pesticide savings through adaptive shut-off logic. The system's modular design also made it applicable to different sprayer architecture and operating speeds, laying the foundation for future real-time motion-aware control systems.

1.5 Research Objectives

This thesis builds on two major experimental studies—each corresponding to a distinct aspect of boom motion.

a). Phase 1: Horizontal Motion and Application Rate Error.

- Quantify horizontal (fore–aft) boom displacement under field conditions using the DQS–GNSS system.
- Convert measured surge velocity into instantaneous application-rate error and aggregate rate-error exceedance boom area under practical error thresholds (±5 %, ±10 %, ±15 %) (shown in 2.3.5).
- Compare stability across three 120-ft sprayers—Hagie STS12, John Deere 412R, and Miller Nitro 7310—operated at multiple speeds (6, 12, 18 mph).
- Evaluate how boom position (front vs. rear), truss material (steel vs. hybrid), and structural configuration affect horizontal stability and rate uniformity.

b). Phase 2: Vertical Motion and Nozzle-to-Canopy Clearance.

- Extend the sensing framework by integrating radar canopy sensors with DQS and GNSS to measure vertical oscillation and canopy response.
- Quantify boom tip displacement, tilt angle, and section-wise nozzle-to-canopy clearance for a 120-ft New Holland Guardian SF310.
- Evaluate height-tolerance exceedance duration within agronomic tolerance bands (±5 in / ±0.127 m and ±10 in / ±0.254 m) (shown in 3.3.7a).
- Assess potential chemical savings using asymmetric shut-off logic (+27 in / –20 in) to estimate reduced active spray time during drift-risk or canopy-contact conditions.

1.6 Scope and Significance

The research presented in this thesis delivers the first detailed, field-scale assessment of both horizontal and vertical sprayer-boom dynamics using an integrated sensing framework. By capturing motion in real time under realistic operating conditions, it quantifies how boom design and terrain interactions influence spraying performance.

The developed DQS–GNSS–radar framework establishes a practical tool for evaluating boom performance and diagnosing instability. Metrics such as rate-error exceedance area, time outside height tolerance, and canopy correlation provide new, quantitative ways to benchmark machine stability and guide improvements in sprayer design, control systems, and application standards. This integrated approach lays the groundwork for future adaptive spraying systems that can maintain accuracy and efficiency across diverse field conditions.

Chapter 2 - Impact of Horizontal Boom Motion on Application Rate Error: Field Evaluation of Three 120-Ft (36m) Sprayers.

2.1 Abstract

Horizontal (fore–aft) boom motion alters nozzle ground speed and can cause localized under- and over-application even when rate controllers maintain the average flow. This study quantified the field-scale impact of horizontal boom instability on application rate error for three commercial 120-ft (36m) self-propelled sprayers: a front-boom Hagie STS12 with a hybrid aluminum–steel truss, a rear-boom John Deere 412R with a steel truss, and a front-boom Miller Nitro 7310 with a full-steel truss. A computer-vision Distance Quantifier System (DQS) integrated with dual-frequency GNSS tracked left-tip displacement at 10 Hz during trials on ~100 acres of post-harvest maize residue near Clifton, Kansas (March–April 2024) with each machine operated at 6, 12, and 18 mph (≈10, 19, and 29 km/h). Maximum fore–aft excursions reached 2.7 m during terrain transitions. A physics-based model converted surge velocity into instantaneous rate error, and dwell-qualified exceedances (≥0.30 s) were aggregated into rate-error exceedance boom area fractions at 5%, 10%, and 15% thresholds. Results showed consistent design-based differences. At the ≥10% error threshold, rate-error exceedance area was ≤2% for both the John Deere rear-boom steel truss and the Hagie front-boom hybrid truss, but 7–10% for the Miller front-boom steel truss. Rate-error exceedance area declined with increasing forward speed (e.g., Miller: 27% at 6 mph vs. 18% at 18 mph), reflecting the inverse scaling of fractional error with travel velocity. Across all conditions, the rear-boom steel John Deere was most stable, the hybrid Hagie was intermediate, and the steel front-boom Miller was least stable. These findings provide the first field-scale evidence linking horizontal boom motion to application performance. They demonstrate that boom architecture—position and material—exerts greater influence on surge behavior than operating speed. Incorporating horizontal motion into sprayer design and performance standards could reduce misapplication bands, improve chemical use efficiency, and enhance agronomic outcomes.

2.2 Introduction

Uniform pesticide application is essential for effective crop protection and input efficiency. When spray distribution is uneven, some areas are under-dosed and pests survive, while others are over-dosed, wasting chemical and risking crop injury. The position and stability of the sprayer

boom strongly influence this uniformity. Vertical boom motion alters nozzle height, which affects droplet drift and canopy coverage; for this reason, most standards and control technologies focus on maintaining vertical boom height (Zhao et al. 2022). Horizontal boom motion(fore–aft) surge operates differently but can be equally disruptive. When the boom tip surges forward, nozzle ground speed increases and the spray pattern stretch, leaving under-sprayed gaps. When the tip lags back, ground speed decreases and spray fans overlap, producing double application (Anglund and Ayers, 2003)(Sharda et al., 2011).

Prior research has approached this problem from different angles where, (Ooms et al. 2002) used GNSS and sensors to measure boom excursions and (Reynaldo et al. 2016) reported oscillation modes across designs. These studies described how much the boom moved but did not connect motion to application error. Other works acknowledged that surge alters nozzle speed and spray distribution (Anglund and Ayers, 2003) and (Sharda et al., 2011) but did not measure boom displacement directly in the field. Recently, (Yan et al. 2021) combined modeling and experimental measurements to characterize boom oscillations and their potential influence on spray uniformity. However, their experiments were conducted on controlled rigs and shorter boom setups rather than full-scale commercial sprayers operating across field terrain. While valuable for understanding vibration mechanics, their work did not provide direct field-scale estimates of application error.

Taken together, prior research either measured displacement without connecting it to rate error or reasoned about application error without measuring motion. Direct field-scale evaluations that integrate both displacement measurement and application error quantification remain very limited. Recent sensing advances have made field-scale quantification feasible. In earlier work (Dalal et al., 2024.), co-authored by the present authors, developed the Distance Quantifier System (DQS), a computer-vision tool integrated with GNSS for measuring boom displacement with 2 cm accuracy. That study validated the system's ability to measure displacement in controlled conditions. What remains unaddressed is translating measured displacement into application error at full scale and comparing how different sprayer architectures influence those outcomes.

(Figure 1) illustrates this mechanism using field data from the Distance Quantifier System (DQS). The center boom GNSS track (blue) follows a steady path, while the tip path (orange) shows fore–aft excursions. During an S-type turn (Figure 1A), tip velocity varied substantially relative to vehicle speed, with forward surges increasing nozzle velocity and backward lags

reducing it. These velocity differences translated directly into spray distribution errors (Figure 1B): forward surges created under-sprayed gaps, while backward lags caused over-applied bands. This example demonstrates how horizontal boom motion, even during moderate maneuvers, can generate localized misapplication.

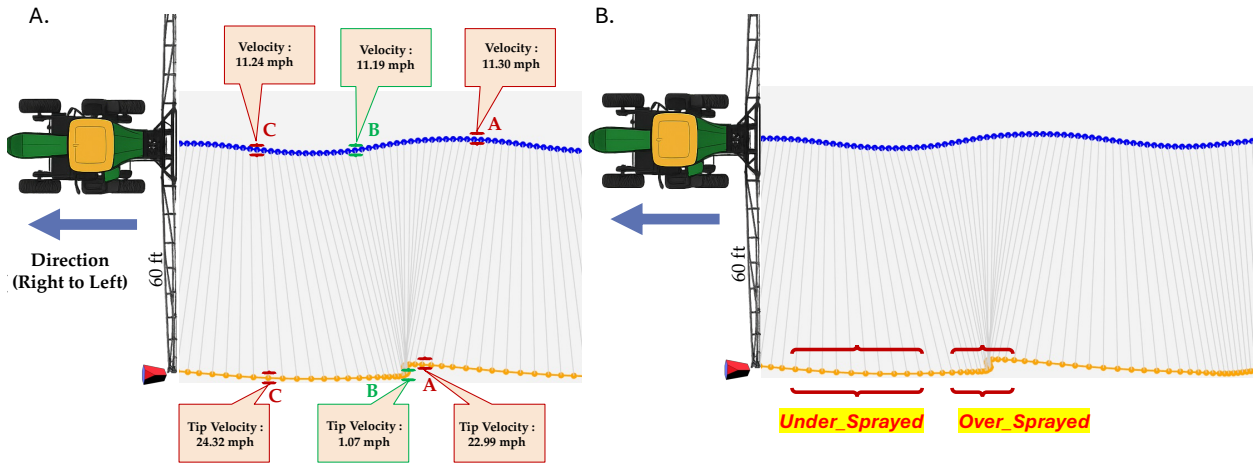


Figure 1: *Example of horizontal boom surge measured in the field. Blue line shows the GNSS track at the boom center; orange line shows the left boom tip path measured with the Distance Quantifier System (DQS). The sprayer image is illustrative. Forward surges increased nozzle ground speed, creating under-spray, while backward lags decreased speed and caused over-application. Direction of sprayer Right to Left.*

A key relationship highlights why this integration matters. Rate controllers set nozzle flow based on vehicle speed, yet a nozzle's true speed is the vehicle speed plus boom surge velocity. From the standard sprayer calibration equation (ASABE EP409.3), the resulting instantaneous application rate error can be expressed as:

$$Rate\ Error = \frac{Vehicle\ Speed}{Vehicle\ Speed + Boom\ Surge\ Speed} - 1$$

This expression shows that for a given boom surge speed (mentioned in 2.3.5), fractional error is amplified at lower travel speeds and diluted at higher speeds.

This study addresses that gap by applying the DQS to three commercial 120-ft sprayers with contrasting designs: a front-boom Hagie STS12 with a hybrid aluminum–steel truss, a rear-boom John Deere 412R with a steel truss, and a front-boom Miller Nitro 7310 with a full-steel truss. Field trials were conducted at three forward speeds (6, 12, and 18 mph) on ~150 acres of Kansas terrain. Boom tip displacement was recorded at 10 Hz, converted into instantaneous rate

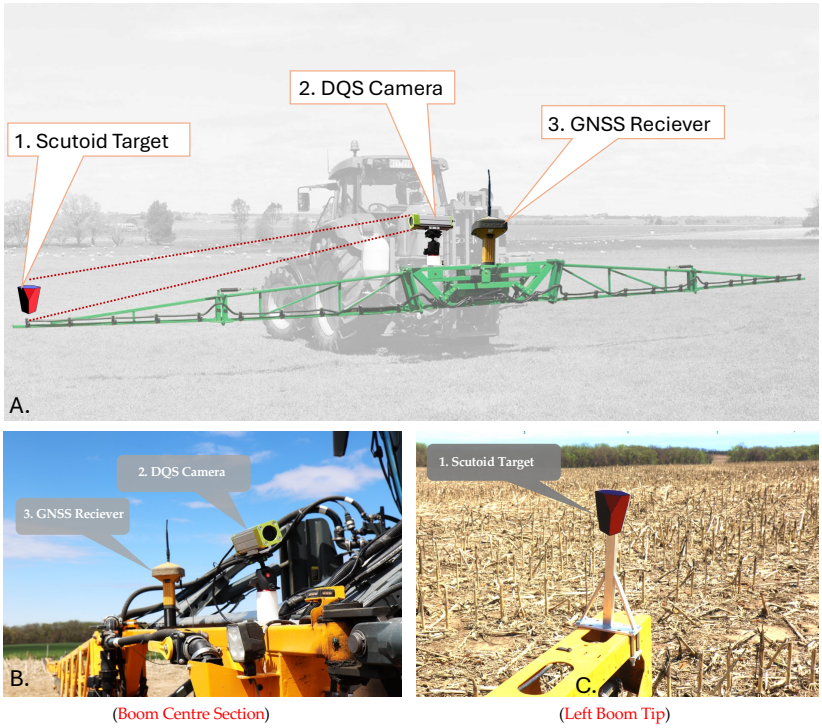
error, and aggregated into rate-error exceedance boom area using practical thresholds. The specific objectives were to:

1. Measure horizontal boom displacement in the field using a vision–GNSS system.
2. Convert motion into nozzle ground speed and application rate error.
3. Compare rate-error exceedance spray area across different boom designs (front vs rear, hybrid vs steel).
4. Examine how forward speed scales error levels.
5. Provide field-scale evidence that boom architecture—position and material—dominates fore–aft stability and should be incorporated into sprayer performance evaluation and design standards.

2.3 Materials & Methods

2.3.1 Distance Quantifier System

A custom made Distance Quantifier System (DQS) (Dalal et al., 2024.)was integrated into a sealed DAQ box mounted on the sprayer. The core instruments included a Topcon GR-5 GNSS receiver operating at 10 Hz (for Position, Speed, and Elevation) and a single industrial camera also operating at 10 Hz, which tracked a scutoid-shaped target on the left boom tip (Figure 2).



(Boom Centre Section) (Left Boom Tip)

Figure 2: ***Setup of the Distance Quantifier System (DQS) on the sprayer boom.***

Camera and Optics.

A Basler ace acA1920-40gc (GigE) camera, which is a color camera and has a has high 1920 * 1200 pixel resolution, equipped with a Kowa 35 mm f/1.4 C-mount lens was housed in a waterproof enclosure and rigidly mounted at the boom center (as boom center is the place of reference with minimum distortion on the boom) on a custom 3D-printed bracket. Camera exposure and gain were fixed for each run, with short exposure times chosen to minimize motion blur.

Fiducial Target.

A high-contrast, scutoid-shaped fiducial tested and developed by (Dalal et al., 2024.) (Scutoid shape was discovered in (Gómez-Gálvez et al., 2018)) was applied to an aluminum bracket bolted to the left boom tip as shown in (Figure 2). The target's edges and vertices provided stable features for tracking across varying viewpoints.

GNSS receiver.

Position, speed, and elevation of the sprayer were recorded using a Topcon GR-5 dual-frequency, multi-constellation receiver operating at 10 Hz. The antenna was mounted at the boom center on a 3D-printed bracket. RTK corrections were applied when available.

Data Acquisition and Computing.

All sensors were integrated into a sealed DAQ enclosure containing a fan-less industrial PC with solid-state storage running a LabVIEW (National Instruments) program. The system provided synchronized acquisition and control, with video inference at 10 fps and raw video recording for offline analysis. All data streams shared a unified system time (s) for cross-referencing.

2.3.2 Experimental Site

Field trials were conducted on ≈100 acres located at 39°20′26.4″ N, 97°10′50.8″ W near Clifton, KS, during March–April 2024. The field was previously planted with maize and contained post-harvest residue but no standing canopy. Elevation across the trial corridors ranged from ≈363 to 385 m above sea level, giving a total relief of about 22 m. Terrain features included flat plains, rolling terraces, waterways and drainage paths, headlands, field entrances with occasional ruts, and cross-slope segments. Tracks were laid out so that each sprayer operated in the same corridors at three different speeds. Start/stop points were marked with flags, and visible crop rows were used

to maintain consistent alignment across passes. Trials were conducted under low-wind conditions to isolate machine- and terrain-induced dynamics.

2.3.3 Sprayers Tested

Three self-propelled 120 ft (36.6 m) boom sprayers (two front boom and one rear boom) were tested by the same professional operator along identical GNSS-guided passes (*Table 1*). The Auto Boom Height Control system was kept enabled on all machines and boom height was kept at 50 inches (1.27 meters) as a safety measure, since the test field included terraces, waterways, and uneven ground where manual control could risk boom damage. To ensure fairness between machines, the sensitivity setting of the Auto Boom Height Control was fixed at 50% for all three sprayers. This provided consistent vertical response while still allowing the natural horizontal (fore–aft) motion of the booms to occur and be captured by the measurement system.



Hagie *STS12* | John Deere *412R* | Miller *Nitro 7310*

Table 1: ***Specifications of Sprayer model used in field trials***

Sprayer	Boom Position	Make/Model	Boom Type	Boom Material	Empty Weight**	Tire Size
FB1	Front	Hagie (STS12)	Truss	Aluminum Hybrid*	12,546 kg	750/60R46 (flotation)
RB1	Rear	John Deere (412R)	Truss	Steel	15,125 kg	650/65R38 (flotation)
FB2	Front	Miller (Nitro 7310)	Truss	Steel	13,471 kg	380/90R50 (row-crop)

**Hybrid Material – Steel inner parts and Aluminum Outer parts to make the boom light.*
***Manufacturer dry weights (empty solution tank); rounded*

2.3.4 Test Protocol

Each sprayer executed a standardized maneuver script at 6, 12, and 18 mph across the 100-acre field in a specific marked track plan (Figure 3). To avoid too much of soil compaction from the sprayers running again on same passes, only one speed pass per track was taken Each pass included steady-state segments plus disturbances: terraces(traversed across and along the

terrace direction), approaches (headland and waterway entry/exit), acceleration(normal/hard acceleration leaving headlands), braking(average/hard braking on straights), and turns(U-turns, boundary turns, S-turns, sharp turns). These maneuvers represent common field disturbances that excite fore–aft boom motion (pitch/surge) beyond steady-state travel.

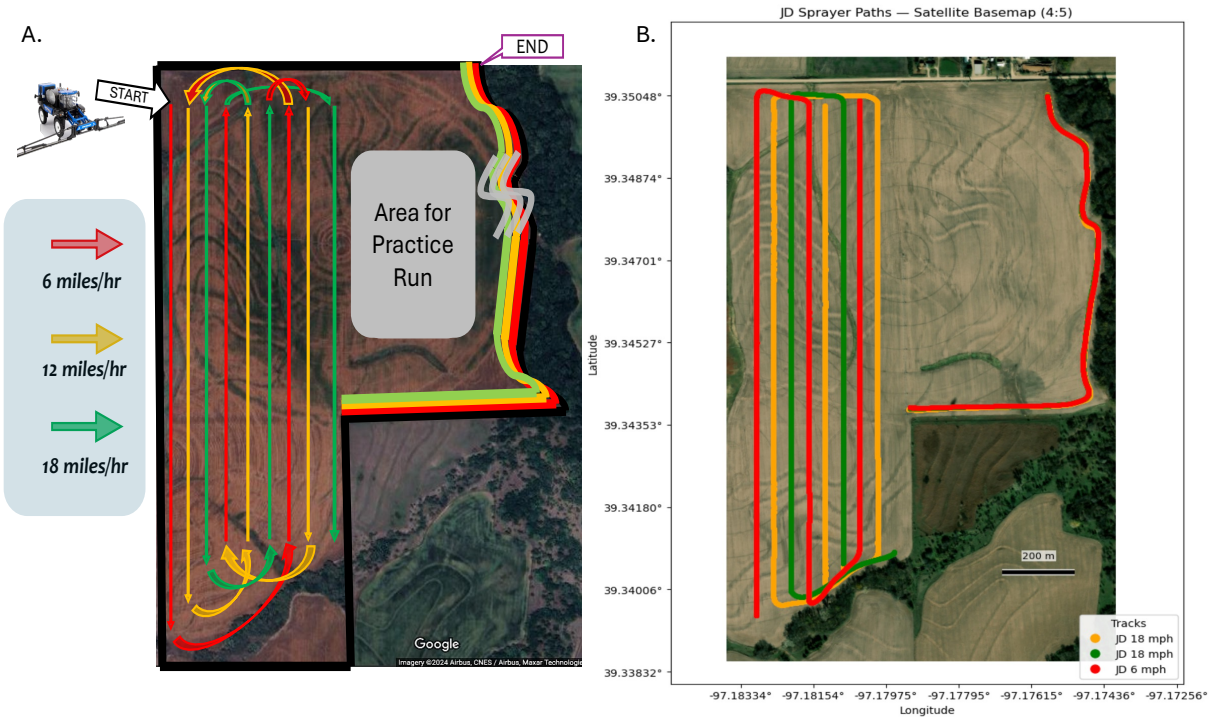


Figure 3: *Planned and actual field trial paths for maneuver testing. (A) Prescribed track plan showing designated corridors for sprayer runs at 6, 12, and 18 mph, with practice run area indicated. (B) Example of an actual GNSS track from the John Deere 412R sprayer following the prescribed course. Disturbance zones included terraces, approaches, braking, acceleration, and turns, designed to excite fore–aft boom motion under realistic field conditions.*

2.3.5 Data Processing

All data were processed in Python 3.11 using pandas, numpy, scipy, and matplotlib. Processing steps are described below.

Step 1: Pixel Detection and Scaling

Each video frame was processed with a YOLO Ultralytics v8 detector trained on >6,500 labeled images of the scutoid target (Dalal et al., 2024.). The detector returned the corner position of the fiducial target in pixel coordinates (x, y).

Pixel displacements were converted to metric displacement using a fixed calibration scale. At the 60-ft (18.288 m) standoff, the field of view equaled 1019.1 mm, which corresponded to

~0.52 mm per pixel at 1920 × 1200 resolution. Centroid shifts were multiplied by this factor to obtain horizontal displacement (fore–aft, x) and vertical displacement (y) in meters. These displacement signals serve the base input for subsequent steps.

Step 2: Unit conversion and outlier filtering

Horizontal Displacement and Elevation values were already in meters(m). Vehicle speed from GNSS was converted from Miles per hour to Meters per seconds. A Hampel filter (10-frame window, 3× median absolute deviation) was used to remove non-physical spikes caused by occasional missed detections.

Step 3: Boom Tip Velocity (fore-aft)

Tip Velocity was calculated as the change in Horizontal displacement (fore–aft, x) divided by the change in time between frames. "GPS Time" from the GNSS receiver was used as the reference time.

$$\textbf{\textit{Boom Surge Speed}} = \frac{\Delta\, \textit{Horizontal Displacement}\ (x)}{\Delta\, \textit{Time}}\ \textbf{(ms}^{-1}\textbf{)}$$

A Savitzky–Golay filter was used to smooth this velocity series and reduce noise while preserving surge events.

Step 4: Application rate error (tip level)

The controller uses the vehicle speed to adjust the nozzle flow, but if the boom tip surges forward or back, the nozzle's true ground speed isn't just the vehicle speed. Then the nozzle's true speed is:

$$\textbf{\textit{Actual Nozzle Speed = Vehicle Speed + Boom Surge Speed}}$$

The Basic Sprayer calibration equation (ASABE EP409.3) says:

$$\textbf{\textit{Target Application Rate}} = \frac{\textbf{5940}\ x\ \textit{Nozzle Flow}\ (Q)}{\textit{Ground Speed x Nozzle Spacing}}$$

Therefore,

$$Q \propto R_{target}\ x\ \textit{Vehicle Speed}$$

So,

$$R_{Actual} \propto \frac{Q}{\textit{Actual Nozzle Speed}} \quad \propto \quad R_{Target}\ x\ \frac{\textit{Vehicle Speed}}{\textit{Vehicle Speed + Boom Surge Speed}}$$

Canceling the proportionality constant gives the clean relation:

$$R_{Actual} = R_{Target} \; x \; \frac{Vehicle\ Speed}{Vehicle\ Speed + Boom\ Surge\ Speed}$$

Application Rate Error goes by:

$$Rate\ Error = \frac{R(Actual) - R(Target)}{R(Target)} = \frac{Vehicle\ Speed}{Vehicle\ Speed + Boom\ Surge\ Speed} - 1$$

$$Rate\ Error = \frac{Vehicle\ Speed}{Vehicle\ Speed + Boom\ Surge\ Speed} - 1$$

Step 5: Setting the Threshold Value for Error & Dwell Time.

To interpret application rate error in terms of practical spraying outcomes, we set three error bands:

- **Warning: |Rate Error| > 5% :** sprayer manufacturers and extension calibration guides often use ±5% as a "good" tolerance band for application rate during steady travel. Exceeding this may still be acceptable short-term but is worth flagging.
- **Rate-Error Exceedance: |Rate Error| > 10%:** Chosen as the primary rate-error threshold because ±10% is a widely accepted tolerance for rate controllers and is consistent with ASABE/extension field evaluations of application uniformity (Sharda et al., 2011).
- **Severe Rate-Error Exceedance: |Rate Error| > 15%:** Represents a severe error. At this level, misapplication is large enough to create visible streaks or over-spray bands, especially with medium droplets.

Droplets need time to fall from the nozzle to the crop canopy. Large droplets (≥400 μm) fall 0.5 m in approx. 0.1–0.3 s. medium droplets (200–240 μm) fall the same distance in approx. 0.7–1.4 s (Nuyttens et al. 2009)(Holterman 2003). Therefore, a surge that lasts less than ~0.30 s is unlikely to persist long enough to shift the spray band by more than a few centimeters. By requiring a dwell time ≥0.30 s (3 frames at 10 fps), we only count surges that are long enough to affect droplet placement on the crop.

Step 6: Nozzle Wise Modelling

For calculating the speed for each nozzle on the boom, we modeled it as a rigid beam rotating about the hinge where its length is 17.678m (58ft), having total of 34 nozzles with a

spacing of 0.508m(20inches). Therefore, for i^{th} nozzle at the distance r_i, its surge speeds were scaled from the tip as:

$$\textit{Nozzle Surge Speed}_i = \frac{r(i)}{L(tip)} \textit{ x Boom Surge Speed}$$

Similarly, the application rate error for the i^{th} nozzle was:

$$\textit{Rate Error}_i = \frac{\textit{Vehicle Speed}}{\textit{Vehicle Speed} + \textit{Nozzle Surge Speed}(i)} \textit{ - 1}$$

Step 7: Distance and Area Aggregation

At each time step Δt, the sprayer traveled:

$$\Delta d = \textit{Vehicle Speed} \times \Delta t$$

If nozzle i was above threshold during that interval, the rate-error exceedance area increment was:

$$\Delta A_i = \Delta d \times \textit{Nozzle Spacing}$$

Summing across time and nozzles gave the rate-error exceedance area per wing. Whole-boom rate-error exceedance area was estimated by doubling the left-wing area (assuming symmetry). The percent of rate-error exceedance area was:

$$\textit{\% Rate-error exceedance area} = 100 \textit{ x } \frac{\textit{Faulty Area}}{\textit{Total Sprayed Area}}$$

2.3.6 Statistical Analysis

Rate-error exceedance boom area at the ≥10% error threshold was analyzed using a two-factor (ANOVA) with sprayer model (Hagie STS12, John Deere 412R, Miller Nitro 7310) and forward speed (6, 12, 18 mph) as fixed factors. Because the experiment was carried out at field scale without within-cell replication, a main-effects-only model was fit, evaluating the average effect of sprayer and speed while excluding the interaction term. ANOVA was implemented in Python (statsmodels, Type II sums of squares) to evaluate the main effects of sprayer and speed. When significant effects were detected, Tukey's Honestly Significant Difference (HSD) test was applied for pairwise mean comparisons at a significance level of $\alpha = 0.05$. This framework allowed direct testing of whether differences in rate-error exceedance area were associated with machine design, operating speed, or both.

2.4 Results & Discussion

2.4.1 XY density scatter plot

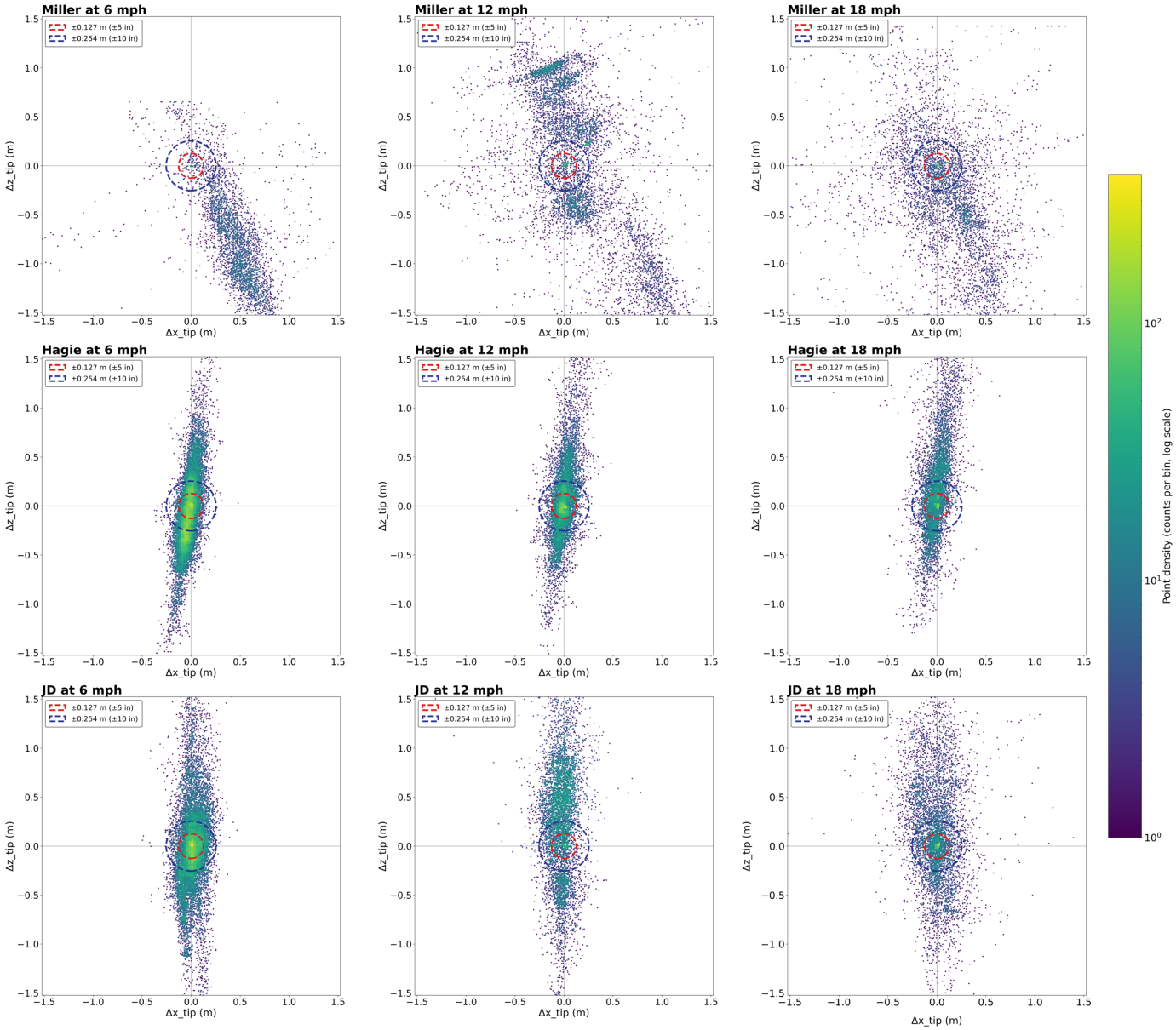


Figure 4: *Boxplots of horizontal (Δx_tip meters) vs. vertical (Δz_tip meters) displacement for all sprayer × speed conditions. dashed circles ±5in /±10in ; crosshairs = stabilized (0,0) start, scatter points show raw displacement.*

The Distance Quantifier System (DQS) captured frame-level horizontal (Δx_tip) and vertical tip (Δz_tip) displacement for all sprayer–speed combinations. (Figure 4) maps boom-tip motion seen by the DQS camera. All panels use the same limits (±1.524 m, ±60″); dashed circles at ±0.127 m and ±0.254 m are quick visual guides, and the crosshairs mark (0,0), defined after ~10 s of steady height before each run. Because rate error comes from fore–aft surge, we focus on

Δx_tip, with Δz_tip shown for context. Miller shows the largest spreads overall: at 6 mph the cloud sits mostly below center with moderate Δx_tip, and at 12–18 mph it fills much of the frame with many visits beyond ±0.254 m. Hagie is vertical-dominant and narrow in Δx_tip—a tall, centered cluster where Δz_tip clearly exceeds Δx_tip. John Deere is vertical-leaning but overall most compact; the cluster stays close to (0,0) with many points inside ±0.127 m.

Clear differences emerged between sprayers as these boxplots provide an immediate visual summary: Miller's motion was dominated by fore–aft oscillations, John Deere showed intermediate stability, and Hagie maintained consistently tight displacement envelopes. This raw displacement visualization also grounds the subsequent rate error analysis in the direct camera measurements.

2.4.2 Boom tip displacement

The DQS system successfully captured fore–aft motion of the boom tips across all sprayers × speed conditions. (Table 2)and (Figure 5) show 95th percentile (P95) displacement values in grouped bar format. Miller Nitro 7310 exhibited the largest surges, with P95 displacement exceeding 1.0 m and RMS >0.5 m at 12–18 mph. Hagie STS12 showed the smallest, most consistent displacements (P95 ≈ 0.18–0.26 m; RMS ≈ 0.12 m). John Deere 412R was small at 6 mph but increased at 12–18 mph (P95 up to ~0.46 m; RMS up to ~0.31 m). These differences might reflect on machine architecture: the rear-mounted steel boom on JD staying intermediate vs the light-weight front-mounted hybrid (steel + aluminum) boom on Hagie, which showed the lowest surges vs the heaviest steel boom on Miller, showing the maximum surges.

Although operator and speeds were matched across runs, we cannot ascribe the between-sprayer differences solely to design. The patterns may reflect architecture, but unmeasured

factors—limited here to tire size and suspension/hydraulic tuning—could also contribute. Accordingly, these results should be interpreted as consistent with, not proof of, design effects.

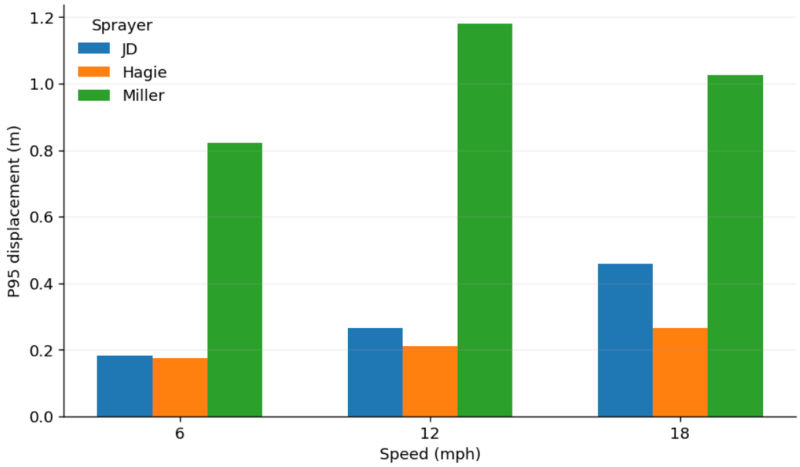


Figure 5: *P95 and RMS fore–aft displacement for each sprayer × speed condition.*

2.4.3 Instantaneous rate error

Instantaneous application rate error was derived from GNSS speed and tip surge velocity. (Figure 6) and (Table 2) shows P95 values of the absolute error distribution. Miller showed up to 66% error at 12 mph were as Hagie stayed ~22–35% and JD ~20–32%. Although mean rate error stayed near zero (controller held average flow), instantaneous excursions matter agronomically. Miller's high tails confirm frequent localized under- and over-application events, even when averages looked correct. This highlights the limitation of relying on mean rate control alone.

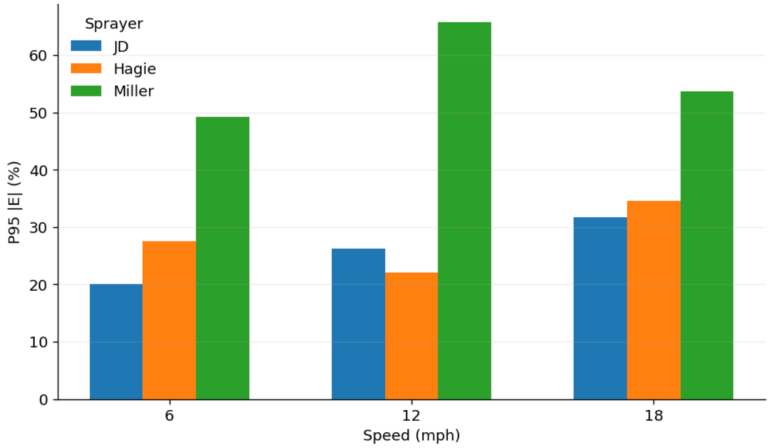


Figure 6: *P95 |E| instantaneous application rate error by sprayer and speed.*

2.4.4 Rate-error exceedance boom area (dwell-qualified aggregation)

Nozzle exceedances persisting ≥0.30 s were aggregated into rate-error exceedance boom area. (Table 2) reports displacement, error, and rate-error exceedance area metrics. Miller Nitro

7310: 7–10% rate-error exceedance area at the 10% threshold. Hagie STS12: ≤2% at 10%, dropping to 0.5% at 18 mph. JD 412R: consistently ≤2%. Rate-error exceedance area converts nozzle surges into field-scale consequences. In a 100-acre field, Miller would misapply ~9 acres, JD ~1.6 acres, and Hagie ~1 acre. Over the 150-acre test site, this equates to ~13 acres for Miller versus ~2 acres for Hagie or JD. This demonstrates the agronomic and economic importance of accounting for horizontal surge.

Table 2: *Statistics Summary Table for rate-error exceedance boom area for the 3 sprayers.*

Sprayer	Speed (mph)	P95 Displacement (m)	RMS Displacement (m)	P95 |E| (%)	Exceedance ≥5% (%)	Exceedance ≥10% (%)	Exceedance ≥15% (%)
Hagie	6	0.175014	0.115049	27.590575	9.268243	1.682028	0.570729
Hagie	12	0.211128	0.120118	22.107720	3.752128	0.842778	0.408038
Hagie	18	0.263910	0.129269	34.612694	3.012727	0.540437	0.224979
JD	6	0.182900	0.091865	20.059480	6.130398	1.000109	0.259855
JD	12	0.265500	0.163975	26.284050	6.535531	1.841924	0.883919
JD	18	0.457250	0.305628	31.637790	6.228830	1.866802	1.001622
Miller	6	0.821372	0.326123	49.261817	27.486400	10.105768	4.855528
Miller	12	1.179325	0.558696	65.684735	19.975745	8.398658	4.465287
Miller	18	1.025917	0.512407	53.651066	18.288123	7.156346	3.639709

2.4.5 Nozzle-wise rate error exceedance

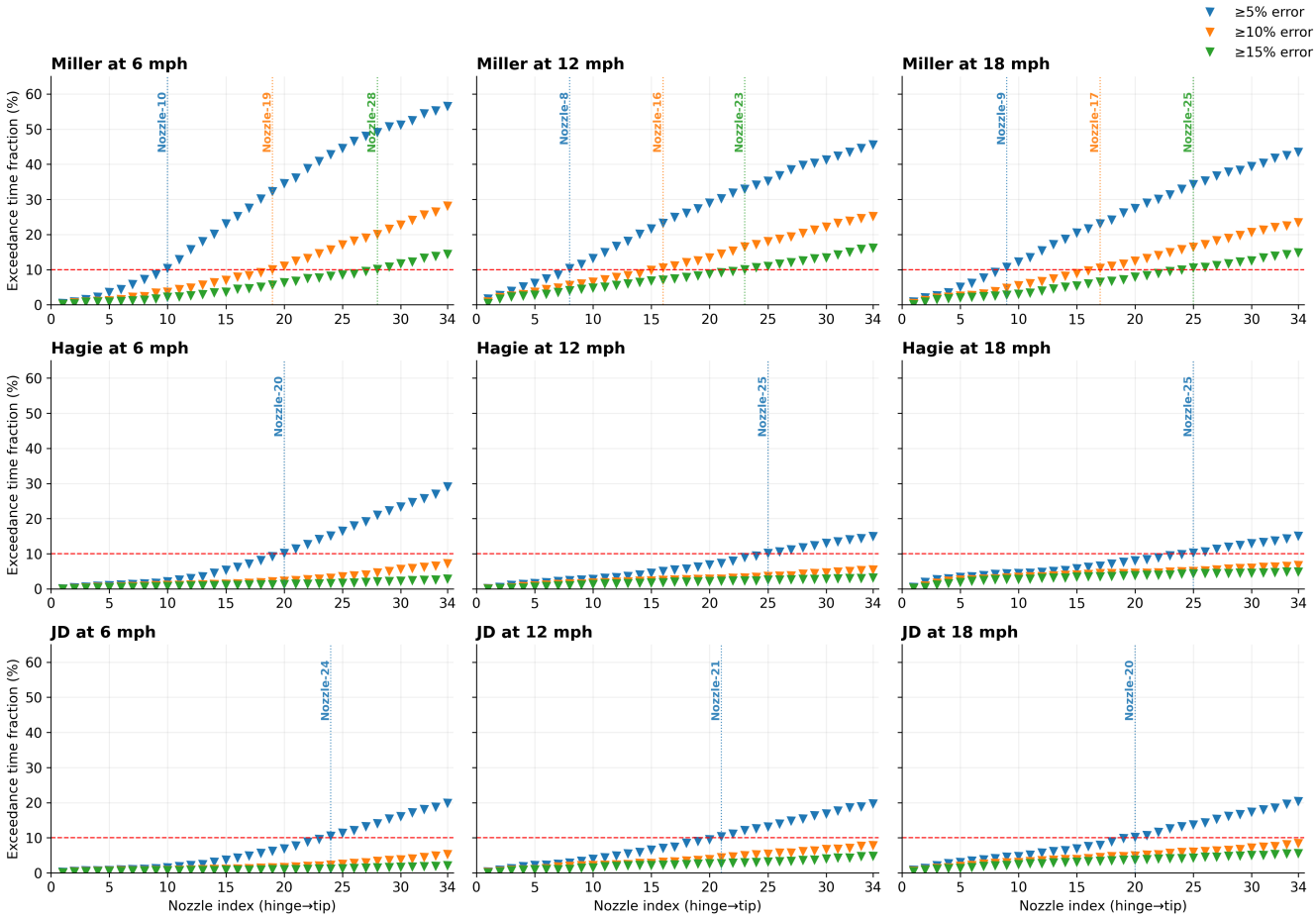


Figure 7: *Nozzle-wise rate error exceedance fractions for the 5%, 10%, and 15% thresholds across sprayers and travel speeds. Each panel shows the fraction of run time that each boom nozzle exceeded a given rate error threshold, with inverted triangles marking individual nozzle positions from hinge to tip. The horizontal red line marks a 10% persistence benchmark common to all sprayers. For each threshold, a color-matched vertical dotted line marks the first nozzle where the exceedance fraction reaches 10%, and the corresponding nozzle index annotated shows the nozzle crossing the 10 % line (for example, "Nozzle-25 in Hagie at 18 mph").*

(

Figure 7) present nozzle-level rate error exceedance fractions across thresholds for each sprayer and speed. These plots reveal how instability propagates along the boom. For Miller Nitro 7310 the rate error exceedance fractions extended deeply into the boom span, with 8–10 nozzles per wing simultaneously exceeding the 10% error threshold at low speed. At 6 mph, surges propagated well beyond the tips, affecting nearly one-third of the span. Even at 18 mph, Miller retained ~6 nozzles consistently above threshold, underscoring persistent instability. Whereas for

Hagie STS12, the exceedances were concentrated near the outer 3–5 nozzles per wing. The inner boom remained stable, showing the hybrid aluminum–steel structure localized but did not eliminate fore–aft oscillations. Hagie showed clear improvement with speed: rate_error exceedance nozzle count dropped by half from 6 mph to 18 mph. In case of John Deere 412R, the rate error exceedance fractions were rare and mostly confined to the outer 1–2 nozzles. The inner 80% of the boom was virtually unaffected, even at 6 mph. This pattern indicates strong damping and decoupling of chassis motion from boom tips.

These nozzle-wise results show that instability is not uniform across the boom. Miller's instability propagated deeply inward the boom while Hagie's and JD's remained localized to tips. Agronomically, this means JD and Hagie errors would cause only tip streaking, whereas Miller could produce broad bands of misapplication.

2.4.6 Sprayer vs sprayer comparisons

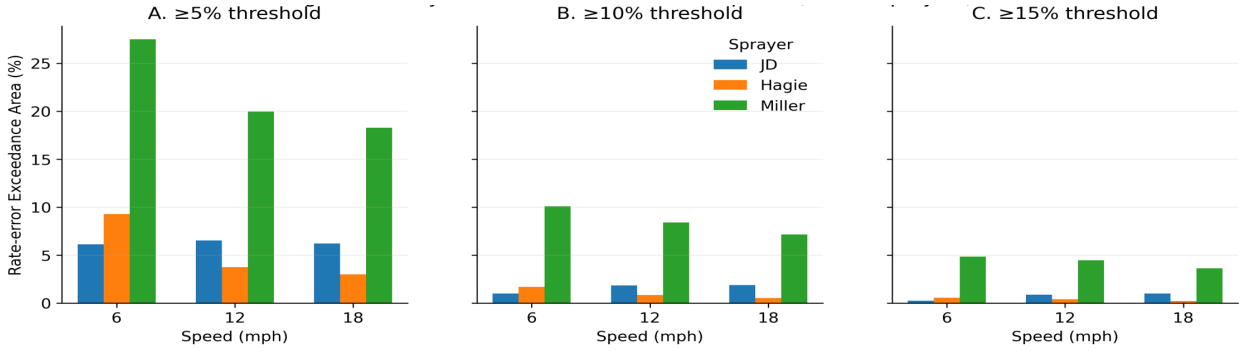


Figure 8: *Rate-error exceedance boom area fractions at 5%, 10%, and 15% thresholds across speeds for each sprayer.*

Figure 8 presents rate-error exceedance area fractions at 5%, 10%, and 15% error thresholds.

- At 5% Miller is highest at all speeds (≈27% at 6 mph, ≈19.5% at 12 mph, ≈17.9% at 18 mph). John Deere stays around 6% at all speeds (≈6.0–6.4%). Hagie drops with speed (≈9.1% → 3.7% → 2.9%).
- At 10%: Miller remains clearly higher (≈9.9% → 8.2% → 7.0%). Hagie is lowest (≈1.64% → 0.83% → 0.53%). John Deere is intermediate and slightly increases with speed (≈0.98% → 1.80% → 1.83%).
- At 15%: Miller is still the only one with notable fractions (≈4.8% → 4.4% → 3.6%). Hagie (≈0.56% → 0.40% → 0.22%) and John Deere (≈0.25% → 0.85% → 0.98%) remain <1% at all speeds.

Miller ≫ John Deere ≥ Hagie overall (John Deere slightly above Hagie at ±10% and ±15%; they are close at ±5%). While the percentages look small, they add up fast in the field. At the ±10% band, a rate-error exceedance of about 7–10% on the Miller boom means roughly 7–10 acres misapplied per 100 acres sprayed. Over 1,000 acres, that is 70–100 acres of under- or over-application—enough to cause visible streaks, wasted product, and potential yield loss. By comparison, the John Deere 412R and Hagie STS12 average about 1–2% and 0.5–1.6%, respectively—still 1–2 acres and 0.5–1.6 acres misapplied per 100 acres (≈ 10–20 acres and 5–16 acres over 1,000 acres). Even at these lower levels, the impact is agronomically meaningful and underscores why limiting horizontal boom surge matters.

2.4.7 Statistical Validation

With one observation per sprayer × speed combination, the design was saturated; therefore, only main effects (sprayer and speed) were tested without interaction. ANOVA results (Table 3) revealed a highly significant sprayer effect ($F = 55.14$, $p = 0.0012$), while speed had no detectable influence ($p = 0.47$).

Table 3: *Two-way ANOVA results for rate-error exceedance area (≥10%).*

Source	Sum Sq	df	F	p-value
Sprayer	105.80	2	55.14	0.0012
Speed	1.73	2	0.90	0.4743
Residual	3.84	4	—	—

Tukey HSD comparisons provided clarity on pairwise differences (Table 4 and Table 5). Sprayer-wise, Miller was significantly worse than both Hagie (+7.53%, $p = 0.0002$) and JD (+6.98%, $p = 0.0003$). The difference between Hagie and JD was not significant ($p = 0.77$). Speed-wise, no pairwise differences were significant ($p > 0.94$).

Table 4: *Tukey HSD post-hoc test (Sprayer, averaged over speeds).*

Comparison	Mean Diff (%)	p-adj	Lower	Upper	Significant
Hagie – JD	0.55	0.7743	-1.87	2.96	No
Hagie – Miller	-7.53	0.0002	-9.95	-5.12	Yes
JD – Miller	-6.98	0.0003	-9.40	-4.57	Yes

Table 5: *Tukey HSD post-hoc test (Speed, averaged over sprayers).*

Comparison	Mean Diff (%)	p-adj	Lower	Upper	Significant
6 – 12	-0.57	0.9855	-11.28	10.14	No
6 – 18	-1.07	0.9495	-11.78	9.63	No
12 – 18	-0.51	0.9885	-11.22	10.20	No

The statistical analysis confirmed that sprayer design was the dominant factor influencing horizontal boom stability, with Miller exhibiting significantly greater rate-error exceedance area than Hagie and John Deere. Tukey HSD comparisons showed Miller exceeded Hagie by 7.5 percentage points and JD by 7.0 points (both $p < 0.001$), while Hagie and JD were statistically indistinguishable. In contrast, speed did not emerge as a significant main effect ($p = 0.47$). Descriptive trends, however, showed that rate-error exceedance area declined with increasing forward velocity, particularly for Miller (27% at 6 mph vs. 18% at 18 mph). This pattern is consistent with the governing relation:

$$\textbf{\textit{Rate Error}}_i = \frac{\textbf{\textit{Vehicle Speed}}}{\textbf{\textit{Vehicle Speed + Nozzle Surge Speed}}(i)} \textbf{\textit{ - 1}}$$

which predicts that higher travel velocity dilutes fractional rate error for a given surge velocity. ***Similar behavior was reported by (Yan et al. 2021), who combined modeling and experimental measurements of sprayer booms and found that while absolute displacement increased with speed, its relative effect on application error diminished***. Taken together, these results indicate that while forward speed influences boom dynamics, its proportional impact on rate error is minor compared to the much larger design-based differences among sprayers.

2.4.8 Sprayer Design Effects

Across all metrics, sprayer design exerted the strongest influence on horizontal stability and application error. The front-boom Hagie STS12 consistently showed the smallest displacement envelopes and the lowest rate-error exceedance area fractions (≈0.5–1.6% at the ±10% band across speeds). The rear-boom John Deere 412R occupied an intermediate position, while the front-boom Miller Nitro 7310 exhibited the largest fore–aft oscillations and the highest rate-error exceedance areas (for example, up to ≈27% at ±5% and ≈7–10% at ±10%). This ranking was robust across thresholds (5%, 10%, 15%), nozzle-wise exceedances, and whole-boom aggregated areas, indicating that structural and layout features of the machines strongly mediate surge behavior.

Several design factors help explain these differences. The rear-boom placement of the John Deere might have reduced pitch–surge coupling from the chassis, limiting amplification of fore–aft oscillations. By contrast, the front-boom configuration of Hagie and Miller directly exposes the boom to vehicle pitching during acceleration, braking, or terrain transitions, increasing surge sensitivity. Within the two front-boom machines, the Miller Nitro's heavier all-steel boom (13,471 kg machine weight, 380/90R50 row-crop tires) was more prone to oscillations than the Hagie's hybrid aluminum–steel truss boom (12,546 kg, 750/60R46 flotation tires), whose lighter construction and wider flotation tires contributed to intermediate stability.

The importance of tire size and track width in transmitting chassis motions to the boom has been previously documented. (van de Zande, Holterman, and Huijsmans 2012) showed that narrower row-crop tires increase oscillations, while flotation tires dampen them by reducing chassis roll and pitch transfer. This is directly consistent with the present findings: the Miller Nitro, equipped with row-crop 380/90R50 tires, showed the greatest instability; the John Deere 412R, with flotation 650/65R38 tires performed almost similar to the Hagie STS12, with flotation 750/60R46 tires, which performed the best overall in this set.

These findings demonstrate that boom architecture and mass distribution dominate fore–aft stability. While speed can scale the fractional error, design determines the baseline susceptibility of the boom to surge motion. In practical terms, design features such as boom mounting position (front vs rear), truss material, suspension damping, and tire configuration must be considered in efforts to minimize horizontal motion. Future sprayer development may benefit from targeted damping or control strategies at the boom tips, which were consistently the most error-prone sections across all designs.

2.5 Conclusion

This study demonstrated that horizontal boom motion can significantly impact application rate accuracy in full-scale field operations. Using a vision–GNSS Distance Quantifier System (DQS), we quantified fore–aft displacement on three 120-ft commercial sprayers and translated surge velocity into rate error and rate-error exceedance boom area. Results showed that the front-boom Hagie STS12 with a hybrid aluminum–steel truss consistently exhibited the lowest rate-error exceedance area (≈0.5–1.6% at the ±10% band), the rear-boom John Deere 412R with a steel truss was intermediate (≈1–2%), and the front-boom Miller Nitro 7310 with a full-steel truss was most unstable, exceeding ≈7–10% rate-error exceedance area at the ±10% band. Although forward

speed scaled error magnitude—with fractional errors declining at higher speeds—the effect was minor compared to design differences. These findings provide the first field-scale evidence linking horizontal surge to application error, highlighting that boom architecture, including mounting position, material, and tires, exerts a greater influence than travel speed.

In future, testing additional sprayer architectures—such as carbon-fiber booms, active suspension systems, and alternative tire configurations—would help isolate the design elements most responsible for horizontal stability. Furthermore, **integrating horizontal motion sensing with rate control systems could enable adaptive correction strategies, moving beyond passive measurement toward active mitigation**.

Chapter 3 - Field-based evaluation of Vertical Motion and Canopy Clearance in a 120-Ft Sprayer Boom using synchronized DQS, GNSS, and Radar Sensors.

3.1 Abstract

Vertical instability of wide sprayer booms remains a significant source of non-uniform pesticide deposition, drift, and canopy contact risk. This study quantified the vertical motion dynamics of a 36.6 m (120 ft) front-mounted boom on a New Holland Guardian SF310 sprayer using a synchronized Distance Quantifier System (DQS), GNSS, and radar canopy sensors under real field conditions with a 14.6-acre pass. The integrated sensing framework reconstructed nozzle-to-canopy clearances across the left boom wing at travel speeds of 6, 12, and 18 mph, enabling section- and wing-level assessment of spray-height deviation within agronomic tolerance bands of ±5 in (±0.127 m) and ±10 in (±0.254 m).

Vertical oscillations were governed by rigid-body pitching about the hinge, with tilt magnitudes exceeding 3° and occasionally peaking at 4.8°. Corresponding RMS and P95 DQS tip displacements reached 0.44 m and 1.07 m, respectively. Strong cross-correlation between mid- and tip-radar signals ($r > 0.85$) confirmed coherent canopy undulations encountered while traversing terrace contours rather than along them. Reconstructed clearances showed that out-of-tolerance-spraying duration increased systematically with speed and lateral distance from the hinge, rising from 37 % to 44 % of total run time under the tighter ±5 in band, and dropping roughly by half under ±10 in. The tip section exhibited the largest deviation (up to 59 % rate error exceedance at ±5 in), while exceedances above the upper limit (>1.96 m) dominated the total out-of-range duration (>10 % at the tip).

Applying the derived height-based shut-off logic ±(27 / 20) in bands to measured out-of-tolerance durations resulted in a 10% reduction in active spray time, saving approximately 5 L of pesticide per boom per pass, equivalent to more than 35 L of savings per 100 acres. These findings confirm that boom vertical motion is primarily hinge-driven and not terrain-following. The developed DQS–radar fusion approach provides a robust foundation for real-time clearance monitoring and adaptive section control, offering a practical route toward more efficient, environmentally resilient spraying systems.

3.2 Introduction

Global pesticide consumption is approximately 3.7 million t yr^{-1} (3.70 Mt in 2022; 3.73 Mt in 2023; FAO, 2024; FAO, 2025), and improper boom height during spraying contributes substantially to off-target drift, uneven deposition, and chemical loss to the atmosphere (Nuyttens et al. 2009)&(van de Zande et al. 2012). Such inefficiencies highlight the importance of maintaining precise boom-height control to achieve uniform canopy coverage and minimize environmental contamination. Even small deviations in nozzle height can alter droplet velocity and impaction energy (Holterman 2003), producing under-coverage in low areas or excessive drift from over-height regions. As sprayer widths and travel speeds continue to increase, the resulting dynamic oscillations amplify these errors, reducing deposition uniformity and application efficiency. Ensuring stable boom height has therefore become a key design and operational objective in precision pesticide application.

Most commercial and academic developments in boom-height control have relied on ultrasonic distance sensors, which measure the distance between the nozzle and the target surface. Ultrasonic sensing performs adequately over uniform canopies such as wheat (Zhao et al. 2022) but loses accuracy in dusty, uneven, or thermally stratified air and when the canopy surface is irregular. Several earlier studies quantified boom vibration or motion using single-modality sensors. (Reynaldo et al. 2016) measured vertical oscillations of three self-propelled sprayers with three RTK-GNSS receivers mounted along the boom, achieving centimeter-level accuracy but without canopy coupling. (Yan et al. 2021) developed a finite-element vibration model validated by an ultrasonic sensor to simulate step-excitation response on a 6 m unilateral boom, whereas (Ooms et al. 2002) fused accelerometer, gyroscope, and ultrasonic signals to characterize horizontal boom motion but under controlled conditions. (Zhao et al. 2022) analyzed single-point ultrasonic measurements over wheat canopy, and field trials by (van de Zande, Holterman, and Huijsmans 2012) correlated spray drift with sprayer speed and boom height using laser and ultrasonic sensing. Although these studies improved understanding of boom motion and drift behavior, they typically lacked multi-sensor fusion or realistic field excitation involving terraces, ploughed soil, and across-slope travel.

Recent advances in computer vision, radar technologies now enable synchronized acquisition of both boom-motion and canopy-profile data. (Dalal et al., 2024) applied a vision-based fiducial marker tracking system to quantify sprayer-boom displacement with centimeter

precision, demonstrating the feasibility of image-based motion reconstruction. Despite these advances, a unified framework that couples structural oscillation, terrain response, and canopy clearance across the full boom span under real operating conditions remains largely absent from existing literature.

Building upon this gap, the present study extends previous horizontal-motion analyses to examine the vertical dynamics of a 36.6 m front-mounted sprayer boom under authentic field excitation. A synchronized sensing framework combining a Distance Quantifier System (DQS) vision module, high-precision GNSS receivers, and canopy-profiling radar sensors was developed to capture both boom motion and surface response. These data streams were fused to reconstruct nozzle-to-canopy clearances along the left boom wing, enabling quantification of tip-motion amplitude and tilt angle, which, when integrated with Radar sensors, calculated out-of-tolerance-spraying duration within agronomic tolerance bands (±5 in and ±10 in).

The objectives of this study were (1) to characterize the vertical dynamics and tilt behavior of 120ft wide front-mounted sprayer boom across representative field speeds(6mph, 12mph, 18mph) using synchronized DQS and GNSS sensing; (2) to construct nozzle-to-canopy clearances and quantify section-wise height-tolerance exceedance duration within defined tolerance bands; and (3) to generate a height-based section shut-off command leading to potential pesticide savings. The proposed approach advances precision-spraying research by linking geometric motion data with agronomic performance metrics, providing actionable insights for original-equipment manufacturers (OEMs) to refine boom dynamics and control architectures. Collectively, these contributions will aim to study oscillations and deposition uniformity, and if implemented, will increase spraying efficiency and reduce both financial and environmental costs associated with over-application and spray drift.

3.3 Materials and Methods

3.3.1 Experimental setup

Field trials were conducted at the Kansas State University North Farm (Manhattan, KS, USA) during spring 2024. The test corridor was located at 39°13′14.26″ N, 96°35′38.80″ W, with elevation ranging from ≈320 to 329 m above sea level, giving a total relief of about 9 m. The experimental area covered ≈50 acres and consisted of a recently ploughed field prepared for planting. Unlike the terrain-rich site described in (Chapter 2) – (2.3.2 Experimental Site) this field did not contain major waterways or headlands but was characterized by broad terraces and wide

cross-slope contours. The sprayer was operated across these terraces rather than along them, so that the boom encountered repeated transverse elevation steps instead of gradual longitudinal slopes. The surface condition was rough due to recent ploughing, with shallow ruts from tillage passes.

3.3.2 Sprayers Tested

The experiments were performed using a New Holland Guardian SF310 self-propelled sprayer equipped with a 120-ft (36.6 m) front-mounted steel truss boom(Figure 9)(Table 6). The front-boom design allowed the Distance Quantifier System (DQS) to be mounted directly at the boom center frame, aligned with a reflective marker fixed to the left boom tip. The boom carried 72 flat-fan nozzles at 20″ spacing, with the left 60-ft wing (36 nozzles) selected for instrumentation and analysis.

The sprayer was fitted with row-crop tires, typical for spring field operations. To prevent ground strikes over terraces and uneven ploughed soil, the boom was operated at a nominal clearance of 50″ (1.27 m) above ground, consistent with safe operating practice. Unlike the study in Chapter 1, the Auto Boom Height Control system was switched off so that natural vertical oscillations could be recorded without hydraulic intervention.

The sprayer was guided by a professional operator following flagged corridors. Automatic GPS guidance was disabled, and the operator maintained manual alignment with the flagged track. This ensured that measured boom motions reflected the true dynamics of machine–terrain interaction rather than smoothing effects from auto-steer corrections.



Figure 9: *Sprayer Specimen - New Holland SF310*

Table 6: *Specifications of Sprayer model used in field trials.*

Sprayer	Boom Position	Make/Model	Boom Type	Boom Material	Empty Weight	Tire Size
FB	Front	New Holland (Guardian SF310)	Truss	Steel	13,471 kg	380/90R50 (row-crop)

3.3.3 Test Protocol

To maintain comparability across speeds, a trial run of the sprayer was first used to establish a dedicated track across the field. This pass compacted the soil along the wheel paths and served as the baseline corridor for subsequent data collection.

Flags were placed at the start and end of the test track to mark measurement boundaries. The sprayer was then operated along the same flagged corridor at three speeds: 6, 12, and 18 mph. These runs corresponded to the first, second, and third passes along the same tire tracks, ensuring that terrain-induced disturbances were consistent between speeds, although some compaction from earlier passes may have modified the response.

The sprayer was operated across a test track of approximately 1.62 km (1,620 m), with the 120 ft (36.6 m) boom covering roughly 14.6 acres per pass. The left boom section analyzed in this study represented about half of the total spray width (≈ 7.3 acres of coverage). Each run began with the sprayer stationary for several seconds to allow sensor baselines to be recorded. The operator then accelerated smoothly to the target speed before entering the flagged test corridor. Data from all sensors were logged continuously throughout the run and stopped once the sprayer came to rest, producing cleanly segmented datasets. Only the left boom wing was instrumented, and the boom height was maintained at ≈50″ to ensure consistent clearance and prevent damage due to boom collision.

3.3.4 Sensors and instrumentation

A GNSS receiver and a Distance Quantifier System (DQS) camera were both mounted at the boom center frame. The GNSS unit provided sprayer velocity, latitude, longitude, elevation, and a GPS-based time base (~10 Hz) for synchronizing all data streams. The DQS camera was aligned with a fiducial marker (scutoid target) fixed at the left boom tip, recording high-frequency vertical and horizontal displacements of the tip relative to the boom center. This configuration, previously used for horizontal motion analysis in Chapter 1, was extended here to study vertical oscillations and tilt dynamics.

The sprayer came equipped with a factory-installed **Raven AutoBoom® XRT** system, which included five radar canopy sensors distributed across the full 120-ft boom used mainly for Auto boom height control as seen in (Figure 10). In this study, only the three sensors on the left boom wing were analyzed, The center radar was fixed near nozzle 1, located 20″ from the hinge.

A second radar was placed midway between nozzles 18 and 19 at 370″ from the hinge. The third radar was mounted directly above nozzle 36 at the boom tip, 720″ from the hinge. These three anchors allowed the canopy surface under the boom to be approximated section by section. The raw distance signals from these radars were accessed via the sprayer CAN bus. All data streams (GNSS, DQS, radar CAN's) were synchronized using the GNSS timestamp.

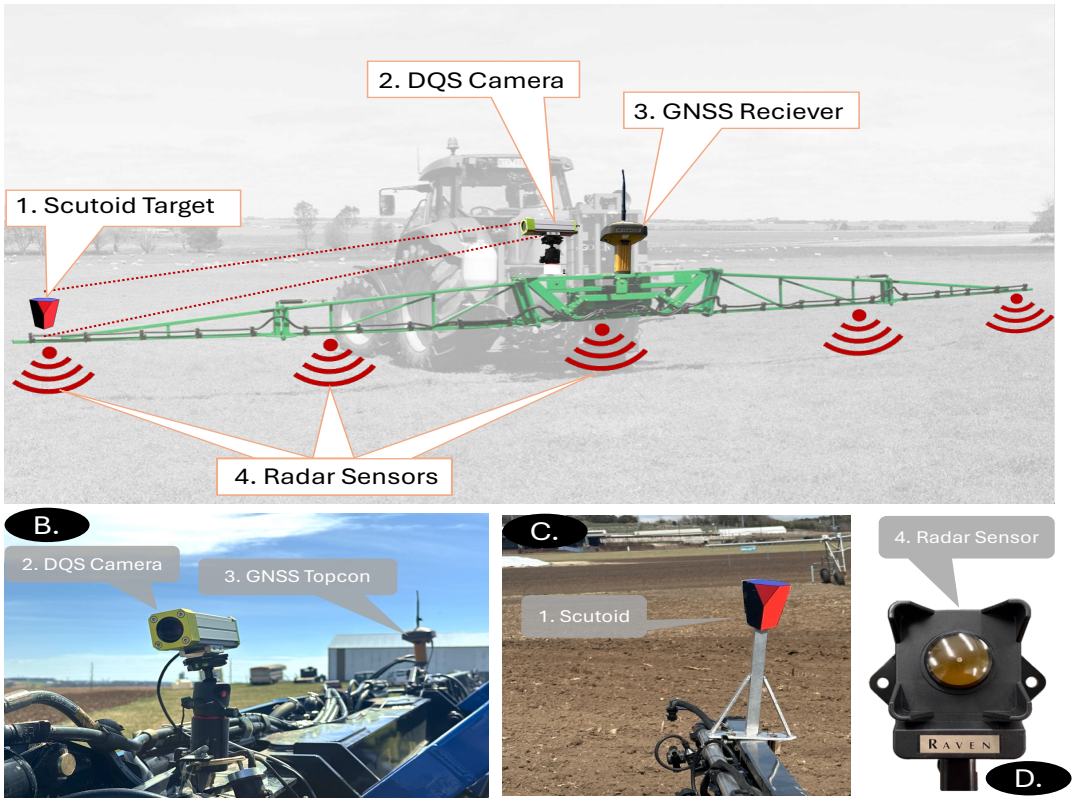


Figure 10: *Setup of the Distance Quantifier System (DQS) on the sprayer boom. (1) Scutoid fiducial target mounted on the left boom tip; (2) DQS camera at the boom center; (3) GNSS-Topcon receiver at boom center; (4) Raven AutoBoom® XRT Radar sensor.*

3.3.5 Radar sensors accuracy check

Prior to field data collection, each Raven AutoBoom® XRT radar was manually verified against measured canopy heights at multiple boom positions (left-tip, mid, and centre). Across five independent tests, the difference between measured and actual canopy distance remained within ±3 cm, confirming the radar system's high accuracy and repeatability under static conditions. This calibration check ensured that subsequent canopy-profile and clearance calculations reflected true geometric distances rather than sensor bias.

3.3.6 Data Processing

The raw signals from the GNSS units, Distance Quantifier System (DQS), and Raven AutoBoom® XRT radar sensors were post-processed to obtain nozzle-to-canopy clearances. The workflow is described step by step below.

a). Baseline reference (DQS initialization)

The DQS camera was activated only after the boom was held stationary at the start line. The first video frame with the scutoid target in view was defined as the reference baseline (0,0). Both vertical and horizontal signals were zeroed at this frame. From this point, all subsequent values represented true displacements of the tip relative to its initial position.

Tip displacement and boom tilt angle

The vertical displacement of the boom tip relative to the baseline was calculated as:

$$\Delta z_{\text{tip}}(t) = Y_{\text{tip}}(t) - Y_{\text{tip}}(0)$$

where:

- $\Delta z_{\text{tip}}(t)$ = vertical displacement of the boom tip at time t, relative to baseline (inches)
- $Y_{\text{tip}}(t)$ = vertical position of the tip measured by DQS at time t (inches)
- $Y_{\text{tip}}(0)$ = baseline vertical position at the start of the run (set to 0)

This displacement was then converted into a tilt angle of the entire boom wing:

$$\theta(t) = \arcsin\left(\frac{\Delta \text{z } tip(\text{t})}{\text{L}}\right),\ L = 720''$$

where:

- $\theta(t)$ = instantaneous tilt angle of the wing (radians)
- $\Delta z_{\text{tip}}(t)$ = tip displacement at time
- L = 720″ = hinge-to-tip distance (60 ft)

b). Sectional grouping of nozzles

The left boom wing measured 60 ft (720″) and contained 36 nozzles, each spaced at 20″ intervals. To enable nozzle-level clearance modeling, the wing was subdivided into three functional sections, each tied to the nearest Raven AutoBoom® XRT radar sensor, as shown in (Figure 11).

- **Centre section (nozzles 1–12):** This block spanned from the boom hinge out to 240″ (≈20 ft). The center radar was mounted directly above nozzle 1, located 20″ from the hinge.

Nozzles in this section were modeled relative to this anchor, with displacement scaled by the tilt angle.

- **Mid-section (nozzles 13–24):** This block extended from 240 inches to 480 inches (≈20–40 ft). The mid-radar was positioned at 370 inches, approximately between nozzles 18 and 19. This allowed it to represent canopy distance near the center of this section, with nozzles on either side interpolated using tilt corrections.
- **Tip section (nozzles 25–36):** This block spanned from 480 inches out to the boom tip at 720 inches (≈40–60 ft). The tip radar was mounted directly above nozzle 36, the last nozzle on the wing. Clearances for all tip nozzles (25–36) were referenced to this radar, with inboard positions adjusted according to boom tilt.

This arrangement provided three canopy anchors across the span, ensuring that canopy variation under the boom was adequately sampled while also capturing the effect of boom tilt. Although only three radars were used, all 36 nozzle clearances could be reconstructed by combining anchor readings with tilt angle geometry.

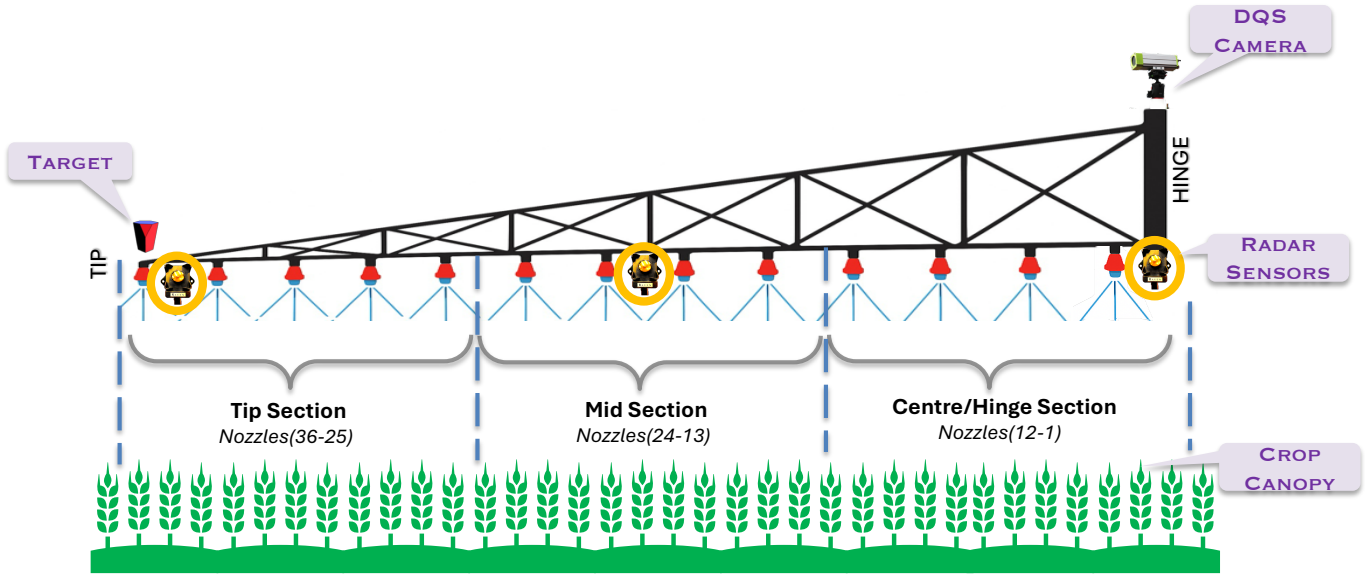


Figure 11: *Sectional Grouping of nozzles.*

This sectional grouping also reflects the physical control structure of modern self-propelled sprayers, where nozzle banks are managed in groups through PWM (pulse-width modulation) or solenoid-based section valves. Each section can be turned on or off as a unit by the rate controller, whereas individual nozzle actuation is uncommon in most field configurations (Sharda et al. 2011)(J. D. Luck et al. 2011). Therefore, evaluating height deviation and time outside height

tolerance on a per-section basis aligns with the machine's actual control architecture and field operation logic.

c). Nozzle-to-canopy clearance modeling

The Raven AutoBoom® XRT system provided canopy distances at three anchor positions (center, mid, tip). Clearances for all 36 nozzles on the left wing were estimated using:

$$H_{\text{noz}}(y, t) = H_{\text{anchor}}(t) + (y - y_a)\sin(\theta(t))$$

where:

- $H_{\text{noz}}(y, t)$ = clearance (inches) between nozzle y and the canopy at time t
- $H_{\text{anchor}}(t)$ = canopy distance measured by the radar anchor at position y_a
- y = lateral position of nozzle from hinge (inches)
- y_a = lateral position of the anchor radar (inches)
- $\theta(t)$ = tilt angle from DQS (radians)

Imagine the boom as a long, rigid plank hinged at the sprayer frame. If the tip goes up, the entire plank rotates around the hinge. At the very end (nozzle 36, where the tip radar is mounted), the nozzle moves the most because it is the farthest from the hinge. That radar gives us the true clearance at the extreme tip. Now look slightly inboard, at nozzle 35. Since it is closer to the hinge, it does not rise as much as the tip during the same tilt. If the boom tilts upward, nozzle 35 will end up a little lower relative to the canopy than the tip, because it didn't "lift" as far. If the boom tilts downward, nozzle 35 will end up a little higher relative to the canopy than the tip, for the same reason.

In other words, the farther out a nozzle is, the bigger its vertical swing when the boom tilts. The closer the nozzle is, the smaller its swing. This method leveraged the rigid-beam geometry of the boom. By combining radar anchor measurements with tilt angle, we reconstructed realistic clearances for all nozzles, even though only three radar sensors were available.

3.3.7 Metrics and statistical analysis

a). Nozzle-level error classification

Each reconstructed nozzle clearance was compared to a fixed target clearance of 50 inches (consistent with the operating boom height during testing). A nozzle was classified as out-of-tolerance when its clearance deviated beyond either ±5″ or ±10″ from the target for a continuous duration (dwell)of at least 0.30 s.

Formally:

$$\textit{Height-tolerance fraction}_{\text{noz}} = \frac{\text{t}(|H\text{noz(t)} - 50| > \text{band})}{T\text{run}} \text{ x } 100$$

Where,

- H_{noz}(t) = nozzle clearance at time t.
- 50 = target clearance (inches).
- band = threshold band (either ±5″ or ±10″).
- T_{run} = total duration of the run (seconds).
- t(.) = total amount of time (in seconds) that the condition inside is true.

The ±5″ and ±10″ tolerance bands represent realistic agronomic limits for nozzle height variation. (Zhao et al. 2022) used comparable criteria of ±10 % and ±20 % when assessing boom-height control performance. Excessive height increases drift potential and reduces canopy coverage, whereas insufficient height increases the risk of canopy contact and localized over-application. A dwell requirement of 0.30 s was applied to exclude short-term signal fluctuations or transient noise from being classified as true errors.

b). Section-level aggregation and Shut Off

These nozzle-level results were averaged across the three functional sections defined in Section 2.5.3. which are Centre (nozzles 1–12), Mid (nozzles 13–24), Tip (nozzles 25–36). This yielded section-level percentages of height-tolerance exceedance, tied to each radar anchor.

A supplementary shutoff analysis was performed to evaluate when individual boom sections would operate outside agronomically acceptable height limits. Although all passes maintained a nominal boom height of 50 in (1.27 m) for measurement consistency, actual field recommendations for 110° flat-fan nozzles specify a target height of ~20 in (0.50 m) above canopy (Kruger, 2019.); (Zhao et al. 2022). To emulate real drift and canopy-contact limits, asymmetric clearance thresholds were applied relative to the 50 in reference:

- Upper limit = +27 in (+0.69 m) → 1.96 m total height (drift-risk boundary)
- Lower limit = –20 in (–0.51 m) → 0.76 m total height (canopy-contact boundary)

Any nozzle section that remained above 1.96 m or below 0.76 m for ≥ 0.30 s was classified as shutoff-worthy. These limits were derived from established drift-height evaluations, which show that boom heights above ≈ approximately 0.9–1.2 m markedly increase off-target drift (Pan et al. 2025) and that excessive lowering (< 0.25 m) can disrupt spray pattern uniformity and risk

canopy strike (Nuyttens et al. 2009). Thus, the asymmetric ±(27 / 20) in envelope provides a conservative, evidence-based operating range for evaluating potential section shutoff triggers.

c). Wing -Level aggregation and Additional motion metrics

Section-level results were further aggregated across all 36 nozzles to compute overall wing-level out-of-tolerance – time percentages under each tolerance band and travel speed. Beyond threshold-based errors, summary statistics including mean, standard deviation, RMS, and P95 values were calculated for each radar and DQS signal. Correlation coefficients between canopy radars (centre, mid, tip) were also computed to assess profile similarity across the boom span. All analyses were performed in Jupyter Notebook using Python libraries such as NumPy, Pandas, Matplotlib, and SciPy. Beyond threshold-based errors, we also calculated:

3.4 Results & Discussion

3.4.1 DQS Tip Vertical Motion



Figure 12: *Time-series of DQS-measured tip vertical displacement (Δz_tip) at three forward speeds (6, 12, 18 mph). The traces share a common vertical scale for comparison. The largest oscillation envelope occurs at 12 mph, indicating resonance-like amplification of boom response.*

The Distance Quantifier System (DQS) camera tracked the left boom tip relative to the boom center across three passes at 6, 12, and 18 mph. (Figure 12) shows the timestamp versus vertical displacement (Δz_tip) in meters (and inches). The 6 mph pass produced the smoothest profile, with oscillations typically contained within ±0.75 m (±29.5 in). At 12 mph, the oscillation

amplitude nearly doubled, with peaks approaching ±1 m (±39.4 in), while at 18 mph the motion became faster but slightly less extreme. (Table 7) summarizes quantitative DQS motion statistics, which shows that the boom tip maintained a slight downward offset (mean Δz_tip = –0.28, –0.42, –0.12 m for 6, 12, 18 mph). RMS and P95 amplitudes peaked at 12 mph (0.61 m and 1.07 m), confirming that vertical motion was greatest at the intermediate speed before damping at 18 mph.

Table 7: *Statistic summary table of DQS vertical (Δz).*

Speed	Mean Δz (m / in)	SD Δz (m / in)	RMS Δz (m / in)	P95 |Δz| (m / in)
6 mph	-0.276 (-10.9)	0.313 (12.3)	0.313 (12.3)	0.731 (28.8)
12 mph	-0.421 (-16.6)	0.441 (17.3)	0.441 (17.3)	1.066 (42.0)
18 mph	-0.115 (-4.5)	0.419 (16.5)	0.419 (16.5)	0.882 (34.7)

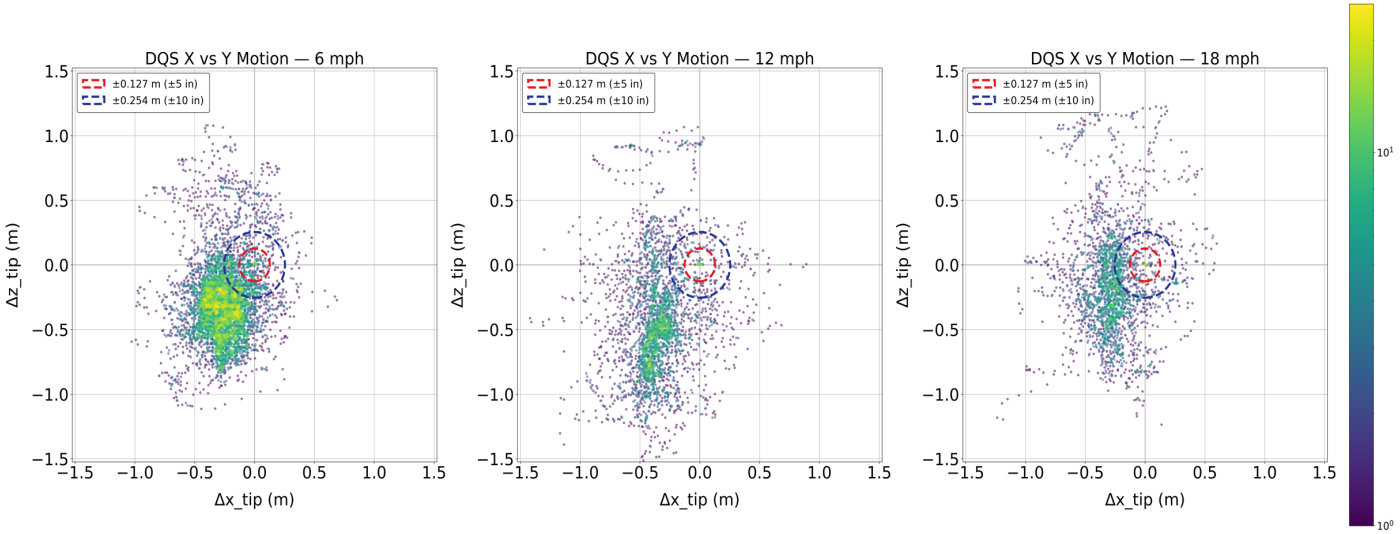


Figure 13: XY *Scatterplots of DQS horizontal versus vertical displacement (Δx_tip vs Δz_tip) for 6, 12, and 18 mph. Shared axes ±1.524 m; dashed circles at ±0.127 m and ±0.254 m; crosshairs = stabilized (0,0) start.*

The DQS scatterplots (Figure 13) shows the boom-tip position seen by the DQS camera at 6, 12, and 18 mph: left–right is fore–aft (Δx_tip) and up–down is vertical (Δz_tip). Dots are colored by how often the tip visited each spot (log density). All three panels share the same limits (±1.524 m, ±60″) for direct comparison. Dashed circles at ±0.127 m (5″) and ±0.254 m (10″) provide quick visual guides, and the crosshairs mark (0,0). As in Section (2.4.1), (0,0) was set after holding the boom steady for ~10 s at the target height, so motion is relative to that stabilized start.

At 6 mph, the cloud is compact and centered near (0,0) with modest fore–aft spread and a slightly taller vertical profile. At 12 mph, the motion expands the most, with a clear vertical elongation and many visits reaching or exceeding the ±0.254 m circle; fore–aft spread also grows.

At 18 mph, the fore–aft spread narrows compared with 12 mph, but vertical tails persist, leaving a taller-than-wide shape. In short, vertical motion (Δz_tip) is consistently larger than horizontal (Δx_tip), peaking at 12 mph. Such behavior is typical of long flexible structures where terrain excitation frequency coincides with the boom's natural oscillatory mode, producing a transient resonance before damping increases at higher speeds. These XY patterns provide the baseline for the height-tolerance exceedance results reported next (time outside the ±5″/±10″ bands).

3.4.2 Radar-Measured Canopy Profiles

Table 8: *Statistic summary table of Radar Sensors (Tip, Mid, Centre).*

Speed	Radar Position	Mean (m / in)	SD (m / in)	RMS (m / in)	P95 Variation (m / in)
6 mph	Centre	1.412 (55.6)	0.082 (3.2)	0.082 (3.2)	0.084 (3.3)
6 mph	Mid	1.389 (54.7)	0.264 (10.4)	0.264 (10.4)	0.552 (21.7)
6 mph	Tip	1.347 (53.0)	0.263 (10.4)	0.263 (10.4)	0.499 (19.7)
12 mph	Centre	1.323 (52.1)	0.097 (3.8)	0.097 (3.8)	0.106 (4.2)
12 mph	Mid	1.367 (53.8)	0.314 (12.4)	0.314 (12.4)	0.682 (26.9)
12 mph	Tip	1.388 (54.6)	0.362 (14.2)	0.362 (14.2)	0.771 (30.3)
18 mph	Centre	1.282 (50.5)	0.111 (4.4)	0.111 (4.4)	0.146 (5.7)
18 mph	Mid	1.377 (54.2)	0.328 (12.9)	0.328 (12.9)	0.625 (24.6)
18 mph	Tip	1.421 (56.0)	0.392 (15.4)	0.392 (15.4)	0.769 (30.3)

The three Raven AutoBoom® XRT sensors recorded canopy distance at the centre, mid, and tip positions. Summary statistics (Table 8) indicates that canopy variation was lowest at the centre (SD ≈ 0.08–0.10 m) and largest at the mid and tip (0.26–0.36 m). P95 values reached 0.50–0.68 m for these outer sensors, showing that terrain undulations intensified away from the hinge.

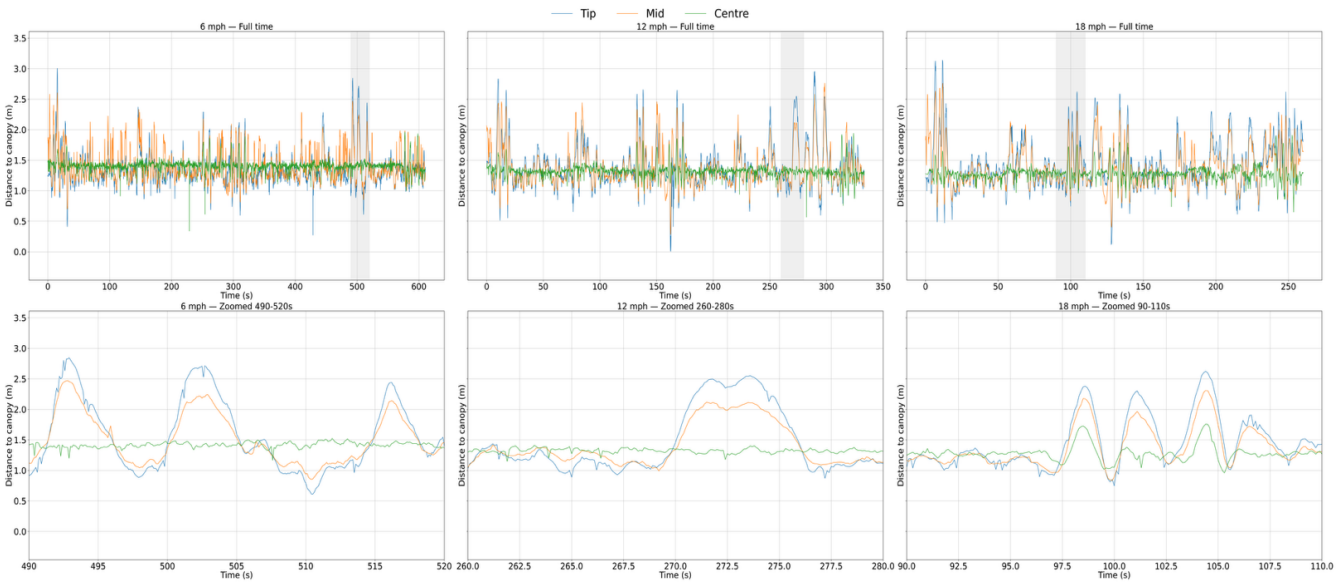


Figure 14: *Canopy distances recorded by the three radar sensors (tip, mid, centre) at 6,12 and 18mph in top row; bottom row shows the zoomed-in view for the same windows to aid curve separation(6 mph: 490–520 s; 12 mph: 260–280 s; 18 mph: 90–110 s).*

Canopy distances measured by the tip, mid, and centre XRT radars are presented in (Figure 14), with the top row showing full-length passages and the bottom row displaying representative zoomed sections (6 mph: 490–520 s; 12 mph: 260–280 s; 18 mph: 90–110 s). All plots share locked Y-scales to emphasize spatial correspondence.

The tip and mid sensors exhibited nearly identical undulations in canopy height, whereas the centre sensor—closest to the hinge—showed smaller variations and a smoother trend. The similarity between tip and mid confirms that the boom was rotating nearly as a rigid body as the canopy variations were primarily transverse (across the slope) rather than longitudinal (along the travel path). Because the hinge is rigidly connected to the sprayer chassis, its motion reflects minimal boom-induced disturbance, meaning that most of the variation observed there originates from the terrain elevation itself. In contrast, the larger oscillations at the mid and tip positions confirm that the boom responded dynamically to terrain excitation.

3.4.3 Radar Cross-Correlation and Boom Motion Statistics

Pairwise Pearson correlations among the three radar canopy-distance signals (Table 9) demonstrate strong coherence between the mid and tip sensors—r = 0.75, 0.89, and 0.89 for 6, 12, and 18 mph, respectively—but only weak correlation between the centre and outer sensors (r ≈ 0.20–0.30). This indicates that the mid and tip followed nearly identical terrain undulations, while the centre radar (closest to the hinge) observed a smoother and slightly offset surface.

The DQS motion amplitudes summarized earlier (Table 7) align closely with these radar trends, confirming that both datasets capture the same tilt-driven, rigid-body boom behavior. As speed increased, motion intensity peaked at 12 mph before moderating at 18 mph—matching the radar-derived coherence patterns and supporting the assumption of rotation about the hinge rather than local flexure.

Table 9: *Pearson correlations matrix summary table of Radar Sensors (Tip, Mid, Centre).*

Radar Pair	6 mph	12 mph	18 mph
Tip – Mid	0.749	0.886	0.885
Centre – Mid	0.211	0.288	0.213
Centre – Tip	0.235	0.248	0.193

The combined radar and DQS evidence show that the boom's vertical dynamics were governed by global pitching motion, not random vibration. The tip and mid-canopy signals rise and fall together ($r > 0.8$), verifying that most displacement arose from hinge-centered rotation. Thus, Tables 1 and 3 collectively establish both the coherence (correlation) and magnitude (RMS/P95) of vertical boom motion, forming the statistical foundation for subsequent clearance and fault analyses.

3.4.4 Tilt Angle Statistics

Using the hinge-to-tip length L = 18.29 m (720 in), instantaneous tilt angles (θ) were computed from DQS tip displacement. (Table 10) summarizes mean, 95th-percentile, and maximum absolute tilt magnitudes for each speed.

Table 10: *Statistic summary table of Tilt angle θ°.*

Speed	Mean |θ|°	P95 |θ|°	Max |θ|°
6 mph	1.13	2.29	3.49
12 mph	1.62	3.34	4.81
18 mph	1.06	2.77	4.33

Typical tilt angles ranged from 1–2° on average, with frequent excursions into ≈ 2.2–3.5° and occasional peaks above 4°, the largest of which was at 12 mph. Although derived directly from tip displacement, tilt provides a normalized and physically interpretable measure of overall boom rotation, essential for nozzle-clearance modeling (Dou et al. 2021)(Yan et al. 2021).

3.4.5 Section-Wise Height-tolerance exceedance

Reconstructed nozzle-to-canopy clearances were compared against the fixed target height of 1.27 m (50 in) using the(3.3.6c)Nozzle-to-canopy clearance modeling). A nozzle was classified as an out-of-tolerance nozzle when its clearance deviated beyond ±5 in (±0.127 m) or ±10 in (±0.254 m) for a continuous duration of 0.30 s or longer.

Table 11: *Section-wise height-tolerance exceedance time (%) under ±5" and ±10" tolerance bands.*

Speed	Section	±5 in (±0.127 m)	±10 in (±0.254 m)
6 mph	Centre	28.46	4.2
6 mph	Mid	39.86	20.86
6 mph	Tip	42.69	17.29
12 mph	Centre	19.22	4.74
12 mph	Mid	48.71	24.4
12 mph	Tip	54.22	31.21
18 mph	Centre	18.53	5.34
18 mph	Mid	54.99	30.83
18 mph	Tip	58.82	37.36

From (Table 11) and (Figure 15), at the tighter ±5 in band, total time outside height tolerance increased from ≈42 % at 6 mph to ≈59 % at 18 mph. The same rank order appeared within each run: Tip > Mid > Centre. When the tolerance widened to ±10 in, fault percentages dropped proportionally (Tip ≈ 17–37 %, Mid ≈ 21–31 %, Centre ≈ 4–5 %), but the spatial ordering remained consistent. At 6 mph and under the wider ±10″ tolerance band, the centre section displayed a slightly higher out-of-tolerance – time fraction relative to its values at higher speeds. This deviation may stem from a combination of factors associated with low-speed boom behavior.

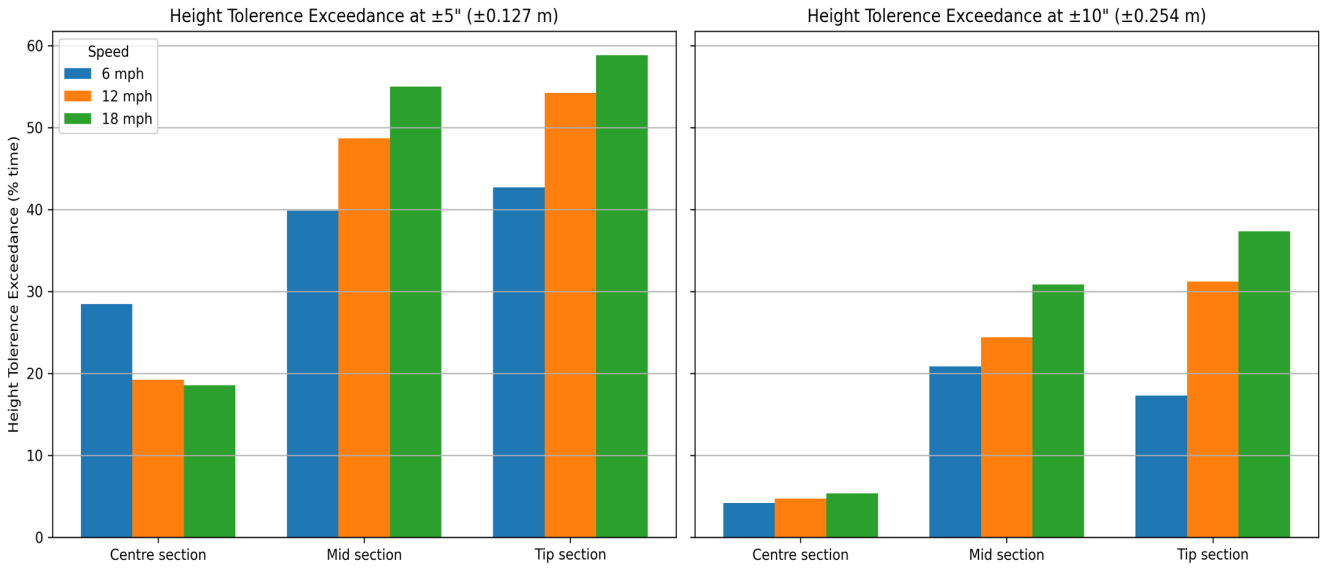


Figure 15: *Bar plots of section-wise height-tolerance exceedance (%) under tolerance bands of ±5" (±0.127 m) and ±10" (±0.254 m). Tip sections consistently exhibit higher time outside height tolerance across all speeds.*

This section-wise trend directly reflects the boom's lever-arm geometry: for a given angular swing, distal nozzles at the tip move through the largest vertical arc, producing longer durations outside the acceptable height band. The smaller deviations at the center arise from its proximity to the hinge, where rotation has minimal vertical effect. Across all sections, time outside height tolerance also rose with forward speed. Faster travel increases the oscillation frequency and shortens the damping intervals, causing the boom to cross tolerance limits more frequently, even when the average tilt remains similar. This behavior aligns with field observations in other boom-height studies, which show that higher operating speeds amplify clearance errors due to dynamic excitation and reduced stabilization times (Dou et al. 2021). Overall, the combined spatial and speed effects suggest that vertical clearance deviations are primarily governed by boom rotation (tilt) rather than canopy interference, with the tip region being most sensitive to small angular changes.

3.4.6 Section Shut Off Command

Table 12: *% time each nozzle section operated outside the set height limits (+27"/-20").*

Speed	Section	Too High > Target +27" (%)	Too Low < Target – 20" (%)	Total Outside (%)
6 mph	Centre	0	0	**0**
6 mph	Mid	3.51	0.13	**3.64**
6 mph	Tip	3.54	0.48	**4.01**
12 mph	Centre	0	0	**0**
12 mph	Mid	6.54	0.24	**6.78**
12 mph	Tip	6.78	1.02	**7.8**
18 mph	Centre	0	0	**0**
18 mph	Mid	5.07	0.27	**5.34**
18 mph	Tip	9.07	1.08	**10.15**

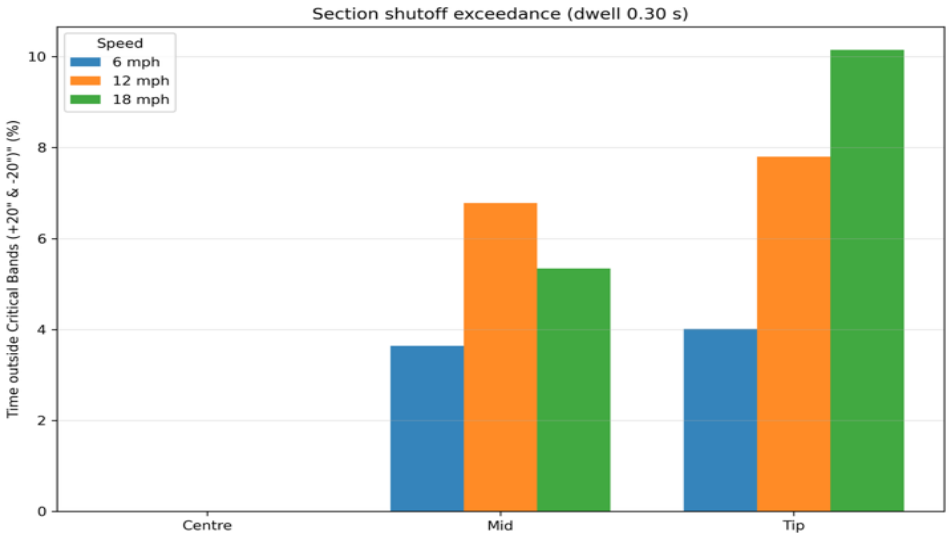


Figure 16: *Section Shutt off % for nozzle sections(Tip, Mid, Centre).*

(Figure 16) & (Table 12) illustrates the duration each nozzle section operated outside the set height limits, where the (Too High > Target +27") column in (Table 8) represents periods when the boom was too high — a situation that increases spray drift risk. The (Too Low < Target – 20") column in (Table 8) represents times when the boom dropped too low, which, in a real field, could cause the nozzles to hit the crop canopy. Because no crop canopy was present during testing, these lower excursions reflect potential impact zones rather than actual contact.

Exceedances above the upper limit were dominant, confirming that boom-tip rise was the primary driver of clearance deviation across all speeds. The total percentage of time outside the acceptable envelope increased consistently with both forward speed and lateral position—rising from ~4 % at 6 mph to over 10 % at 18 mph in the tip section.

Lower-limit exceedances were rare (< 1.1 %), but in a true field scenario would correspond to physical canopy strikes or localized over-application zones. Integrating such asymmetric thresholds (+27″ / –20″) into adaptive section-control algorithms would allow real-time automatic shutoff during drift-prone or contact-risk intervals, improving both spray efficiency and environmental safety.

3.4.7 Wing-level height exceedance summaries

When aggregated across all 36 nozzles on the left boom, the results represent the total time outside height tolerance for the entire wing rather than per-section averages. Across speeds, total time outside height tolerance increased systematically with forward velocity and decreased as the tolerance band widened (Table 13) & (Figure 17).

Table 13: *Wing % time outside height tolerance vs Speeds.*

Speed	Wing Error % (±5″ / ±0.127 m)	Wing Error % (±10″ / ±0.254 m)
6 mph	37	14.12
12 mph	40.72	20.12
18 mph	44.11	24.51

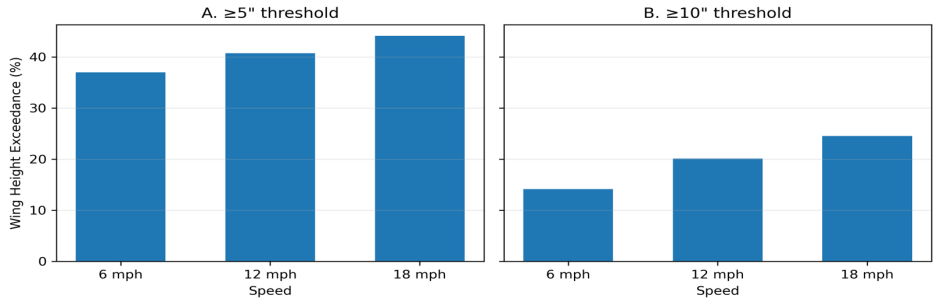


Figure 17: *Wing-level time outside height tolerance (%) versus speed under three tolerance thresholds (±5", ±10"). Fault percentage increases with speed and decreases as the band widens.*

These percentages represent the fraction of total run time during which at least one nozzle on the wing operated outside the specified clearance band. The steady increase in time outside height tolerance with speed shows that higher travel velocity amplifies boom motion, increasing the duration during which the wing departs from its target height. Relaxing the tolerance from ±5″ to ±10″ reduced time outside height tolerance by roughly half, emphasizing that apparent boom-stability performance depends strongly on the agronomic clearance criterion applied. Because the

left and right wings are geometrically identical, these findings are representative of full-boom behavior.

3.5 Conclusion

This study quantified the vertical motion dynamics of a 36.6 m (120 ft) front-mounted boom on a New Holland Guardian SF310 sprayer using synchronized DQS vision, GNSS, and radar canopy sensors under controlled field conditions. The integrated sensing framework successfully reconstructed nozzle-to-canopy clearances across the left boom wing, enabling section-level and wing-level evaluation of spray-height deviations under realistic operating scenarios.

Boom tip displacement and radar-derived canopy motion confirmed that vertical oscillations were governed by rigid-body pitching about the hinge rather than passive terrain following. The largest angular excursions occurred when tilt magnitudes frequently exceeded 3° and occasionally peaked above 4.8°, corresponding to DQS-measured RMS and P95 tip displacements of 0.44 m and 1.07 m, respectively. Strong cross-correlation between the tip and mid-radar sensors ($r > 0.85$) validated the radar system's consistency and confirmed coherent canopy undulations encountered as the sprayer traversed across terrace contours rather than along them. In contrast, the center radar, positioned close to the hinge, exhibited a smaller amplitude and weaker coupling to the outer sensors, consistent with reduced vertical motion and structural damping near the boom pivot.

Reconstructed nozzle-to-canopy clearances revealed that the magnitude and frequency of height-tolerance exceedance increased systematically with both travel speed and lateral distance from the hinge. Within the ±5 in tolerance band, total time outside height tolerance for the wing rose from 37 % to 44 %, while relaxation to ±10 in reduced these fractions roughly by half. Section-wise analysis revealed that the tip consistently exhibited the highest deviation, reaching up to 59% rate error exceedance under the tighter ±5% tolerance band, highlighting its susceptibility to small angular variations in boom tilt. The supplementary asymmetric shut-off analysis confirmed that exceedances above the upper limit (too-high condition) dominated the total out-of-range time, reaching more than 10 % of the run at the tip section.

Applying the derived shut-off logic to the measured out-of-tolerance durations indicates a meaningful reduction in potential pesticide waste. Considering full-wing dynamics, if automatic section shut-off were engaged whenever the boom exceeded the defined asymmetric height limits,

total active spray duration could be reduced by approximately 10 %. At a nominal nozzle flow rate of 0.7 L min^{-1}, this corresponds to nearly 5 L of chemical saved per boom per pass. **When extrapolated to 100 acres of field coverage, the cumulative savings would exceed 35 L of pesticide, representing an 8–12% reduction in total chemical use while simultaneously minimizing drift and canopy-contact risk.** These estimates highlight the tangible agronomic and environmental benefits that can be achieved through sensor-based height feedback and intelligent section control.

Collectively, the results demonstrate that boom vertical behavior is strongly influenced by operating dynamics and geometric distance from the hinge, with rigid-body pitching as the dominant motion mode. The proposed DQS–radar fusion approach provides a robust framework for evaluating nozzle-level clearance errors and for developing adaptive control algorithms that integrate height sensing with real-time section management. ***Incorporating real-time DQS-based feedback into section-control logic could allow dynamic shut-off of drift-risk or canopy-contact zones, offering a path toward more intelligent and environmentally resilient spraying systems.***

Chapter 4 - Conclusion

4.1 Summary of Findings

This research examined how the motion dynamics of wide sprayer booms affect pesticide/fertilizer application uniformity and efficiency under real operating conditions. By integrating computer vision, GNSS, and radar sensors, a complete measurement framework was developed to quantify boom movement and its direct impact on spray performance. The work was carried out in two complementary phases: horizontal motion analysis and vertical clearance assessment.

The first phase focused on horizontal (fore–aft) boom motion, using a Distance Quantifier System (DQS) paired with a dual-frequency GNSS receiver to track tip displacement on three 120-ft commercial sprayers with different designs ran on same passage for 3 different speed(6,12 & 18 mph). Field runs over approximately 100 acres revealed clear contrasts in stability among the machines. The front-boom Hagie STS12 showed the most stable performance, with mean surges small (P95 ≈ 0.18–0.26 m) and rate-error exceedance area ≈0.5–1.6% at the ±10% band. The rear-boom John Deere 412R was intermediate (P95 up to ≈0.46 m; ≈1–2% at ±10%). The front-boom Miller Nitro 7310, with its heavier all-steel truss, exhibited the largest surges (P95 exceeding 1.0 m at higher speeds) and rate-error exceedance areas ≈7–10% at ±10%.Statistical analysis confirmed that boom design and mounting position were far more influential than travel speed, which had only a mild scaling effect on surge amplitude. These results provided the first full-scale evidence that structural configuration directly determines rate-error magnitude, even when automatic controllers maintain target flow.

The second phase expanded this sensing framework by integrating radar canopy sensors with the existing DQS–GNSS system to capture vertical (up–down) motion and nozzle-to-canopy clearance. Tests on a New Holland Guardian SF310 120 front-boom sprayer showed that vertical motion was dominated by hinge-centered pitching rather than terrain following. The boom frequently tilted by more than 3°, with peaks approaching 4.8°, corresponding to 0.44 m RMS and 1.07 m P95 tip displacements. Fault analysis showed that height deviations became larger and more frequent as travel speed increased—from 37 % rate error exceedance at 6 mph to 44 % at 18 mph within the ±5 in (±0.127 m) tolerance band. When the tolerance was relaxed to ±10 in (±0.254 m), the out-of-tolerance – time fractions were cut roughly in half. The tip section, farthest from

the hinge, remained the most unstable, exceeding 59 % rate error exceedance under the tight ±5 in band, while the center section was the most stable. When a height-based section shut-off logic (+27 in / −20 in) was applied, the results indicated an average 10 % reduction in active spray time, equivalent to chemical savings of about 5 L per boom per pass or more than 35 L per 100 acres of field operation.

Together, these findings establish that both horizontal and vertical instabilities meaningfully alter spray uniformity, but for different reasons—horizontal motion stems primarily from boom architecture and mass distribution, while vertical deviation reflects terrain-induced pitching. The developed multi-sensor framework successfully linked these dynamic patterns to measurable agronomic effects, offering a repeatable method to assess boom performance and identify opportunities for motion-compensated spraying.

4.2 Practical Implications

The results of this research demonstrate that boom motion—both horizontal and vertical—has a measurable and direct effect on spray uniformity, chemical efficiency, and drift potential. Even when automatic rate and height controllers maintain average setpoints, rapid dynamic movements can cause local over- or under-application, underscoring the need for real-time motion awareness in modern spraying systems.

From an engineering perspective, boom architecture emerged as the dominant factor influencing horizontal stability. The Hybrid (Steel + Aluminum) front boom Hagie STS12 exhibited minimal surge and the lowest rate error, while the heavier, front-mounted heavy steel boom Miller Nitro 7310 experienced pronounced motion and higher rate-error exceedance areas were as the rear-mounted John Deere 412R steel boom stayed intermediate. These contrasts indicate that design elements such as mounting position, material stiffness, and weight distribution directly determine surge behavior. Manufacturers can use these insights to optimize boom geometry, damping, and support structures for improved stability and reduced rate error.

For field operators and agronomists, he vertical-motion findings demonstrate the agronomic cost of small height deviations. Even a modest increase in boom height can elevate drift risk or reduce canopy coverage, while excessive lowering may cause canopy strikes and over-application. Applying section-level shut-off logic based on measured height limits in the New Holland study demonstrated a potential reduction of about **10%** in active spray duration. When extrapolated to full-field operation, this corresponds to an estimated saving of roughly **5 L of**

chemical per boom per pass, or more than **35 L per 100 acres**, highlighting the broader economic and environmental value of adaptive height management.

The integrated DQS–GNSS–radar framework developed in this research provides a foundation for adaptive spraying systems capable of detecting and compensating for motion in real time. By converting motion data into clear performance indicators—such as time outside height tolerance or section deviation—creates a common language for engineers, manufacturers, and researchers to evaluate boom stability. Together, these implications point toward the next generation of precision sprayers that are not only automated but truly intelligent, capable of maintaining accuracy, reducing waste, and improving environmental stewardship.

4.3 Future Work

- Develop and test real-time feedback control algorithms that use DQS–GNSS–radar data for automatic height and rate adjustment during operation.
- Combine motion measurements with spray deposition and drift modeling to quantify how dynamic errors affect chemical distribution and canopy coverage.
- Expand testing to different canopy types and slope conditions to evaluate framework adaptability under varied agronomic scenarios.
- Validate the vertical-motion framework across multiple sprayer designs and terrains to assess how boom geometry and mounting position affect pitching behavior.

References

Anglund, E A, and P D Ayers. “Field Evaluation Of Response Times For A Variable Rate (Pressure–Based And Injection) Liquid Chemical Applicator.”

Bockhop, Theodore Bryan. 2024. “Characterization and Analysis of an Off-Road Vehicle Hydraulic Lift Arm Suspension.” Master of Science. Iowa State University. doi:10.31274/td-20240617-178.

Dalal, A. S., S. Rai, R. Singh, T. S. Kaloya, R. H. Cheppally, and A. Sharda. 2025. “Computer Vision based Automated Quantification of Agricultural Sprayers Boom Displacement.” CoRR abs/2506.19939. doi:10.48550/arXiv.2506.19939.

Dou, Hanjie, Songlin Wang, Changyuan Zhai, Liping Chen, Xiu Wang, and Xueguan Zhao. 2021. “A LiDAR Sensor-Based Spray Boom Height Detection Method and the Corresponding Experimental Validation.” *Sensors* 21(6): 2107. doi:10.3390/s21062107.

Herbst et al. 2015. “A Method for Testing Automatic Spray Boom Height Control Systems.” In *2015 ASABE International Meeting*, American Society of Agricultural and Biological Engineers. doi:10.13031/aim.20152150720.

Holterman, H. J. 2003. Kinetics and evaporation of water drops in air. IMAG rapport 2003-12. Wageningen, The Netherlands: IMAG, Wageningen University & Research. doi:10.18174/562300.

J. D. Luck, A. Sharda, S. K. Pitla, J. P. Fulton, and S. A. Shearer. 2011. “A Case Study Concerning the Effects of Controller Response and Turning Movements on Application Rate Uniformity with a Self-Propelled Sprayer.” *Transactions of the ASABE* 54(2): 423–31. doi:10.13031/2013.36445.

J. J. Langenakens, H. Ramon, and J. De Baerdemaeker. 1995. “A Model for Measuring the Effect of Tire Pressure and Driving Speed on Horizontal Sprayer Boom Movements and Spray Pattern.” *Transactions of the ASAE* 38(1): 65–72. doi:10.13031/2013.27813.

Kruger, G. R., R. N. Klein, C. L. Ogg, and B. C. Vieira. 2019. Spray Drift of Pesticides (G1773). NebGuide G1773. Lincoln, NE: University of Nebraska–Lincoln Extension. (Originally published 2007, revised 16 Oct 2019.)

Langenakens, Jan J., Luc Clijmans, Herman Ramon, and Josse De Baerdemaeker. 1999. “The Effects of Vertical Sprayer Boom Movements on the Uniformity of Spray Distribution.” *Journal of Agricultural Engineering Research* 74(3): 281–91. doi:10.1006/jaer.1999.0464.

Miles, Lucas. 2018. “Developing General Procedure to Quantitatively Analyze Boom Height Control Performance on Self-Propelled Agricultural Sprayers.” Master of Science. Iowa State University, Digital Repository. doi:10.31274/etd-180810-6043.

Nation, H.J. 1982. “The Dynamic Behaviour of Field Sprayer Booms.” *Journal of Agricultural Engineering Research* 27(1): 61–70. doi:10.1016/0021-8634(82)90058-0.

Nuyttens, David, M. Schampheleire, Pieter Verboven, Eva Brusselman, and Donald Dekeyser. 2009. “Droplet Size and Velocity Characteristics of Agricultural Sprays.” *TRANSACTIONS OF THE ASABE* 52: 1471–80. doi:10.13031/2013.29127.

Ooms, D., F. Lebeau, R. Ruter, and M.-F. Destain. 2002. “Measurements of the Horizontal Sprayer Boom Movements by Sensor Data Fusion.” *Computers and Electronics in Agriculture* 33(2): 139–62. doi:10.1016/S0168-1699(02)00006-6.

Ooms, D., R. Ruter, F. Lebeau, and M.-F. Destain. 2003. “Impact of the Horizontal Movements of a Sprayer Boom on the Longitudinal Spray Distribution in Field Conditions.” *Crop Protection* 22(6): 813–20. doi:10.1016/S0261-2194(03)00045-0.

Pan, Xiaoyong, Shuo Yang, Yuanyuan Gao, Zhichong Wang, Changyuan Zhai, and Wei Qiu. 2025. “Evaluation of Spray Drift from an Electric Boom Sprayer: Impact of Boom Height and Nozzle Type.” *Agronomy* 15(1): 160. doi:10.3390/agronomy15010160.

Pochi, D., and D. Vannucci. 2002. “PM—Power and Machinery: A System with Potentiometric Transducers to Record Spray Boom Movements under Operating Conditions.” *Biosystems Engineering* 82(4): 393–406. doi:10.1006/bioe.2002.0090.

Reynaldo, Étore F., Thiago M. Machado, Leandro Taubinger, and Dionathan De Quadros. 2016. “Vertical and Horizontal Oscillation of Three Models of Self-Propelled Boom Sprayers.” *Revista Brasileira de Engenharia Agrícola e Ambiental* 20(10): 941–45. doi:10.1590/1807-1929/agriambi.v20n10p941-945.

Sharda, Ajay, John P. Fulton, Timothy P. McDonald, and Christian J. Brodbeck. 2011. “Real-Time Nozzle Flow Uniformity When Using Automatic Section Control on Agricultural Sprayers.” *Computers and Electronics in Agriculture* 79(2): 169–79. doi:10.1016/j.compag.2011.09.006.

Tahmasebi, M., R. A. Rahman, M. Mailah, and M. Gohari. 2012. “Sprayer Boom Active Suspension Using Intelligent Active Force Control.” *International Journal of Mechanical and Mechatronics Engineering* 6(8): 1517–1523. (World Academy of Science, Engineering and Technology, Issue 68.

Yan, Junchao, Xinyu Xue, Longfei Cui, Suming Ding, Wei Gu, and Feixiang Le. 2021a. “Analysis of Dynamic Behavior of Spray Boom under Step Excitation.” *Applied Sciences* 11(21): 10129. doi:10.3390/app112110129.

Van de Zande, Jan, HJ Holterman, and J.F.M. Huijsmans. 2012. *Spray Drift for the Assessment of Exposure of Aquatic Organisms to Plant Protection Products in the Netherlands : Part 1: Field Crops and Downward Spraying*. doi:10.13140/RG.2.1.2860.1848.

Zhao, Xueguan, Changyuan Zhai, Songlin Wang, Hanjie Dou, Shuo Yang, Xiu Wang, and Lipin Chen. 2022. “Sprayer Boom Height Measurement in Wheat Field Using Ultrasonic Sensor:

An Exploratory Study." *Frontiers in Plant Science* 13: 1008122. doi:10.3389/fpls.2022.1008122.

Gómez-Gálvez, P., P. Vicente-Munuera, A. Tagua, C. Forja, A. M. Castro, et al. 2018. "Scutoids Are a Geometrical Solution to Three-Dimensional Packing of Epithelia." Nature Communications 9: 2960. doi:10.1038/s1467-018-05376-1.

ASABE. 2010. ASABE EP409.3: Design, Calibration, and Operation of Sprayers. St. Joseph, MI: American Society of Agricultural and Biological Engineers.

FAO. 2024. Pesticides use and trade 1990–2022. FAOSTAT Analytical Brief No. 89. Rome, Italy: Food and Agriculture Organization of the United Nations.

FAO. 2025. Pesticides use and trade 1990–2023. FAOSTAT Analytical Brief No. 109. Rome, Italy: Food and Agriculture Organization of the United Nations.